

Transparent Surfaces Inspired by Nature

Mahdi Motamedi, Majid Ebrahimi Warkiani, and Robert A. Taylor*

Nature has long inspired scientists and engineers. As one ubiquitous example of this, nature has provided all with several clever methods to absorb, repel, and/or allow both sunlight and water to pass through surfaces. Moth's eyes (highly antireflective) and lotus leaves (highly hydrophobic and self-cleaning) represent durable natural surfaces which exhibit nearly ideal physical and optical properties. Man-made transparent surfaces must also be able to cope with water and dust while reaching the maximum possible light transmission for solar collectors, displays, and other optical devices. To explore the link between these – particularly for transparent surfaces – this review puts the physics, progress, and limitations of synthetic materials in context with natural materials. This perspective reveals that there is still much more to learn (and implement) if it is hoped to match the multifunctionality and resilience of natural materials.

of most plant leaves selectively absorbs only part of the visible spectrum – while at the same time being selectively impermeable to water. While water rolls-off tree leaves during rain storms, a tree uses these same leaves to transpire many times its own weight in water (during the growing season) back to the environment via pores found on the underside of most leaves. At the same time, green leaf appears green because the green portion of sunlight is scattered away, while the rest of the visible spectrum penetrates into the depth of the leaf where it can be absorbed by chlorophyll and other photosynthetically active pigments. The transparent thalli of ordinary green algae and the leaves of aquatic angiosperm also selectively utilize visible light.^[1] Butterfly wings cope with

1. Introduction

When light or water interacts with a surface, the surface may repel them, absorb them, or allow them to freely pass through, to varying degrees. Since life on Earth is exposed to both light and water continuously, the outer skin of many flora and fauna species exhibits properties which can manage these elements effectively. Many plants, insects, and even some larger animals have come up with some extraordinary evolutionary optical and/or hydrodynamic adaptations to enable them to thrive in different habitats and/or camouflage themselves from their predators and/or prey. While seemingly mundane, the surface

water by repelling it while selectively reflecting light. Since butterflies do not need light for energy, they have found a more sophisticated optical mechanism to achieve bright, iridescent surfaces (via angular, spectral, and even polarization-dependent surface reflectivity). The *Argyrophorus argenteus* butterfly, in particular, provides a shimmering, iridescent silver and gold example of this via scales on its wings which enable broadband reflectance.^[2] Sphingid moths, satyrids, and ithomiid butterflies also have specular optical properties based on the surface structure and materials that comprise their wings. The “Glasswing butterfly,” the *Greta oto* member of the Ithomiini tribe, provides another interesting example as its highly transparent wings consists of sub-micrometer protrusions which prevent light scattering to reduce their visibility to predators.^[3] Even the more common, Cicada, also has wings with antireflective nanostructures which serve as camouflage.^[2]

Using a different “ordered” mechanism, the corneal surfaces of some insects and butterfly wings include nanometer scale, patterned structures which give these surfaces broadband antireflectivity.^[4] In fact, most moths, *Drosophila* (i.e., fruit flies) and a few species of butterflies, have antireflective eye structures which allow them to gather more light and enhance their sight in low light conditions.^[5] The underlying structure of these surfaces most commonly includes arrays of cylindrical nodules configured in a hexagonal arrangement.^[6] As such, the “moth's-eye pattern” has since been duplicated by several researchers in the lab to develop highly antireflective structures.^[7]


As a mechanically tough example, windowpane oysters are permeable to water and transmit nearly 80% of visible light.^[8] Likewise, some freshwater arthropods, such as the cranchiid squid (*Taonius pavo*) and the hyperiid amphipod crustacean (*Cystisoma*), use transparency as camouflage.^[9]

M. Motamedi, Prof. R. A. Taylor
School of Mechanical and Manufacturing Engineering
University of New South Wales (UNSW)
Sydney, NSW 2052, Australia
E-mail: robert.taylor@unsw.edu.au

Dr. M. E. Warkiani
School of Biomedical Engineering
Center for Health Technologies
University of Technology Sydney
Sydney, Ultimo NSW 2007, Australia

Dr. M. E. Warkiani
Institute of Molecular Medicine
Sechenov First Moscow State University
Moscow 119991, Russia

Prof. R. A. Taylor
School of Photovoltaic and Renewable Energy Engineering
University of New South Wales (UNSW)
Sydney, NSW 2052, Australia

 The ORCID identification number(s) for the author(s) of this article can be found under <https://doi.org/10.1002/adom.201800091>.

DOI: 10.1002/adom.201800091

In addition, several natural surfaces selectively reflect or transmit light based on its polarization. Special chitin molecules found on beetles from the genus *Chrysina* exhibit polarized reflection from bright green to metallic silver-gold.^[10] Akerlind et al. studied the cuticle of *Cyphochilus insulanus*, a scarab beetle, which exhibits a very high reflectance (up to 75%) from 400 to 1600 nm, but outside of this “window” (i.e., in the UV and IR regions), the reflectance is below 20%. Their report also showed that for oblique angles of incident light, this beetle strongly reflects linearly polarized light (noting that light reflected from the surface of lakes and ponds is largely polarized).^[2] Since modern applications require polarizing and wavelength selective filters, there are many man-made materials which have used essentially the same mechanisms to achieve similar (or even better) properties as these natural examples.^[11]

1.1. Modern Light Management Needs

When light lands on any object or medium (natural or man-made), it can be transmitted, absorbed, or reflected. Thus, for high transmission, reflection and absorption must be minimized. Although antireflective coatings might occasionally be used on opaque surfaces/substrates, in practice, they are most commonly placed on transparent substrates (namely glass). Particularly in applications where there is an air/substrate interface, an antireflective (AR) coating represents a means to substantially increase the total amount of light that is transmitted through the AR-coated substrate versus an uncoated substrate. For windows, displays, solar collectors, and fiber optics, transmission is desired, while reflection and absorption are detrimental. In the absence of an AR coating, fused silica glass reflects 4–100% of incident light from its top surface (depending on the incidence angle).^[12] In many applications (e.g., photovoltaics^[13] and micro/nano-electromechanical system devices^[14]), every percentage point of loss in total transmission can significantly reduce performance and functionality. In some cases, reflection can cause complete failure of the material for its application. **Figure 1** shows some characteristic examples of unwanted reflections.

Employing AR coatings, however, can reduce normal incidence reflection to well below 1% in pristine laboratory materials.^[15] For comparison, the wings of the hawkmoth, *Cepho-nodes hylas* have a reflectance of less than 2% over the range of 200–800 nm.^[16] While nature has employed this phenomenon for quite some time, AR coatings have only recently been finding their way into a wide range of modern applications, including: photovoltaic (PV) cells and solar thermal collectors,^[17] television screens/monitors,^[18] light-emitting diodes (LEDs), windows,^[19] photonic crystals (PCs),^[20] biomedical devices,^[21] optical biosensors,^[22] lenses,^[23] lasers,^[24] and many other applications, as shown in **Figure 2**.

1.1.1. Clear and Transparent Materials

Although many modern materials require reduced reflection of visible light (e.g., wavelength ranging from 380 to 700 nm),



interests include green energy, material science, and engineering for solar applications.

Mahdi Motamedi, coming from a biochemical engineering background, joined Prof. Robert Taylor's Group at the UNSW as a PhD student in 2016 to work on a multidisciplinary research related to solar thermal technology. This opportunity enabled him to transition to optics and solar energy research. His current research



USA). He is also a member of Institute for Biomedical Materials & Devices (IBMD) and Center for Health Technologies (CHT) at the UTS, a visiting scientist at the Garvan Institute for Biomedical Research, and a member of the Translational Cancer Research Network (TCRN).

Majid Ebrahimi Warkiani is a Senior Lecturer in the School of Biomedical Engineering, University Technology Sydney (UTS), Sydney, Australia. He received his Ph.D. in Mechanical Engineering from the Nanyang Technological University (NTU, Singapore), and undertook postdoctoral training at the Massachusetts



Robert A. Taylor received his Ph.D. in 2011 from the Arizona State University in the School for Engineering of Matter, Transport, and Energy. His main research interest is in the development of “next-generation” solar thermal collectors. Drawing on the fields of heat transfer and nano-technology, he is researching new/novel working fluids and materials for solar systems.

this represents only a small part of the whole electromagnetic spectrum. However, since our eyes are only sensitive to this small portion of the spectrum, we commonly define “transparent” materials to be those which have very little absorption, reflection, and scattering in the visible region.^[25] For “clear” window and display glass, this definition may indeed be sufficient, since the intended application needs only delivering visible light to human eyes. However, for materials which interact with the full solar spectrum (≈ 250 –4000 nm) or even broader electromagnetic radiation, the word “transparent” should



Figure 1. Examples of unwanted reflection. a) Reflection of sunlight off a solar thermal collector. b) Unclear public transport bus route number due to reflection. c) Photolithography fabrication errors due to reflection/refraction: (1) UV exposure, (2) the exposure result in the absence of bottom antireflective coating (BARC), and (3) the result in the presence of BARC.

be more inclusive. Using a broader definition, typical “clear” window glass is actually opaque since it contains enough iron and other impurities to absorb most of the UV (e.g., <400 nm) and IR (e.g., >1500 nm) spectrum (see **Figure 3a**). Glasses with metal impurities can be thought of not just as insulators, but also as very wide-bandgap semiconductors, wherein the bandgap is too large to absorb much of the visible spectrum (with a large value of E_g in **Figure 3b**).^[26,27] Depending on the number of added impurities (e.g., free electrons/holes), insulators can be made to act more like semiconductors and, similarly, semiconductors can be heavily doped to act more like metals when interacting with light.^[26,27] This control and balance over the optoelectric properties of materials is, of course, the key to obtaining electricity from photovoltaics. An analogous, albeit more circuitous, multistep process which involves trace metals to control light absorption is also the

key to photosynthesis. That is, the active metal atoms in the organic pigments of plant cells enable sunlight to be converted to chemical energy in photosynthesis.^[28]

Transparent conductors, on the other hand, use a different mechanism from semiconductors. In transparent conductors, high frequency/energy incident light, above the so-called “plasma frequency” (e.g., visible light), can be transmitted through the material due to the fact that the electrons cannot respond fast enough. Incident light with a frequency/energy level below this plasma frequency (e.g., IR light), however, is reflected and/or absorbed. This plasma frequency can (again) be tuned through the addition of impurities, but the absorbing/reflective tuning range is usually limited to the near-infrared region.^[29]

Although the base material and its level of impurities play the dominant role, the thickness and crystallinity of the material



Figure 2. Summary of the applications of AR coatings – from large scale (leftmost hexagons) to the small scale (rightmost hexagons).

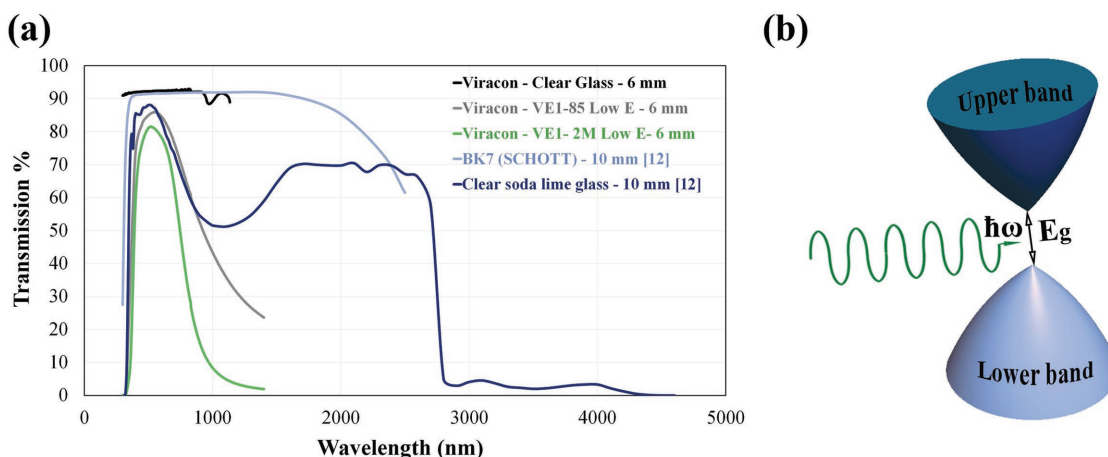


Figure 3. a) Transmission of some commercially available glasses. b) Interband optical excitation between an occupied lower band to an empty upper band. Excitation occurs in (b) if the photon energy, $\hbar\omega$, exceeds the energy difference between the two bands, E_g (the bandgap).

both help to determine the level of transparency. For instance, materials such as glasses and polymers can be transparent in an amorphous state but opaque when crystalline.^[26] Metal films can also be used as transparent conductors if they are “ultrathin”^[30] (e.g., their thickness is in the range of 1–100 Å^[31]).

1.1.2. Clear and Present Progress

Due to the fact that transparency is a property that gets more complicated the deeper one looks, it is often oversimplified. Thus, this review will first provide a brief summary of the fundamental physics involved that must be understood—and invoked—to achieve highly transparent materials. Next, the development of AR coatings will be discussed, focusing on key fabrication and design aspects, including a concise discussion of material selection and deposition methods. Since there are many commonalities in terms of surface structure and chemistry, this review will also discuss self-cleaning surfaces. In addition, several other salient functions that can be beneficially added to AR materials will be discussed. Finally, some key commercial aspects, such as durability and cost, will be considered.

These aspects are timely and important for discussion in this review because our ability to make transparent surfaces has advanced nearly in lockstep with our understanding of natural materials. The underlying mechanisms for the self-cleaning surfaces commonly found in nature (e.g., the lotus leaf^[32,33] and the rice leaf^[34]), insects (e.g., water strider^[35]), and larger animals (e.g., mallard drake or wild duck^[36]) were only discovered in recent decades. Man-made self-cleaning surfaces and “superhydrophobic” surfaces (details discussed below), have only recently been developed in the laboratory (e.g., in the 1990s and early 2000s), and have only very recently combined with AR coatings. According to a historical Scopus search in March 2018, the number of studies which consider both AR and self-cleaning has risen from nearly zero in the year 2000 to ≈10 studies per year by 2010, and may reach ≈20 per year in 2020. We believe this growth could be accelerated further if researchers looked to nature for inspiration.

We hope that this review will reveal that: 1) nature has done a lot to inspire and aid us in creating better transparent surfaces, and that 2) there is still a lot to learn from nature in creating reliable and cost-effective multifunctional, transparent surfaces – materials which maintain high transparency and materials which are imbued with other energy and mass transfer benefits to fit their applications.

1.2. Transparent Materials and Their Applications

Transparent materials are often found in nature, albeit less often than opaque materials. Several animals (e.g., glasswing butterflies,^[37] Antarctic icefish,^[38] jellyfish,^[39] glass octopuses,^[40] glass frogs^[41]) and minerals (diamonds, quartz, and other crystalline gemstones) exhibit some amount of transparency. In man-made materials, transparent substrates have gone from rare to nearly omnipresent in human life. Prior to the industrial revolution, the production of glass and transparent polymers was expensive and limited to relatively small scales due to fabrication issues (e.g., material purity and furnace temperature/size limitations^[42]). However, transparent materials are now a cornerstone of many human industries. Most modern buildings and consumer products include one or more of the following as a critical element: windows, optical filters, lenses, or transparent plastic covers, all of which must transmit light.^[43] Glass, in its various formulations, is the dominant transparent material in these applications, due to its thermal and chemical stability.^[44] That said, in some applications, transparent conductive plastics are relatively of low cost and provide an even wider range of desirable properties (flexibility, low density, manufacturability, thermal and electrical conductivity, corrosion resistance, mechanical toughness, along with more exotic properties like birefringence and biodegradability). Plastics are generally not considered as thermally and/or electrical conductive materials. However, depending on the application, plastics can be made/modified to show transparency together with either one or both thermal and electrical conductivities. Claus and Liu patented a transparent plastic which was thermally and electrically conductive.^[45] Kang et al. fabricated polymer–metal hybrid electrodes which were made antireflective by using a conducting

polymer coating. Their electrodes showed high transmittance of visible light for use in flexible electronic applications.^[46] As such, transparent plastics have become indispensable in many modern products. Implantable medical devices, interactive electronics, military equipment, and robotic systems can all utilize lightweight, transparent transistors and transparent active-matrix circuits.^[47] For flexible, portable electronic devices, transparent plastics can even be coated with transparent conductive oxides – a technology which will soon enable many new commercial gadgets, including flexible touch display panels, steerable antennas, embedded heaters and defrosters, wrap-around heads-up displays, and see-through structural health monitors.^[48,49] Although the number of transparent materials and fabrication techniques may be growing exponentially, they can all be quantified and compared in terms of their transmittance (T) (which is a specular and an angle dependent property) between 0 and 1.

$$T = \frac{P}{P_0} \quad (1)$$

where P_0 and P are light intensity which hits a surface and transmitted by the surface, respectively.

1.3. Achieving Maximum Transparency

As mentioned above, light striking a surface can be transmitted, reflected, or absorbed. Thus, by decreasing the absorptivity, α (i.e., the fraction of light absorbed at a given wavelength), and the reflectivity, ρ (i.e., the fraction of light reflected at a given wavelength), the transmissivity, τ (i.e., the fraction of light transmitted at a given wavelength), can be maximized, as per the following equation^[50]

$$\alpha + \rho + \tau = 1 \quad (2)$$

Since it is relatively easy to minimize absorptivity in modern synthetic materials, gains in transmissivity are more likely to come from obtaining low reflectivity. Reflectivity, in turn, is fundamentally limited by the step change(s) in refractive index (n) when light propagates from air ($n \approx 1$) into a solid material ($n > 1$), and back out (in some applications). The real part of the refractive index, n , is defined by the ratio of the speed of light in vacuum, c , to the speed of light in the current medium, v . Our eyes are actually very good at discerning even small changes in the refractive index (e.g., the interface between oil ($n = 1.47$) and water ($n = 1.33$)) from the way light appears to bend at the interface. The complex part of the refractive index, k , is known as the extinction coefficient. The extinction coefficient is the quantity which controls absorptivity. Our eyes are also very good at discerning changes in the extinction coefficient (e.g., low concentrations, hundreds of parts per millions of smoke or dust particles are visible in air). Pulling together the real and the imaginary parts, the full refractive index, N , can be defined as the following^[51]

$$N = \frac{c}{v} = n - ik \quad (3)$$

It should be noted that the sign convention is not the same across fields – in the thin film community, refractive index is

written as above,^[11] but in physics and other fields, the convention of N or $\tilde{n} = n + ik$ is used.

When the refractive index is known, reflection and transmission can be found from the Fresnel equations. Overlooking absorption (e.g., assuming $k = 0$), the reflectance of a single-layer AR coating in air as the medium can be calculated using

$$R = \left(\frac{n_{\text{air}} n_{\text{substrate}} - n_{\text{AR coating}}^2}{n_{\text{air}} n_{\text{substrate}} + n_{\text{AR coating}}^2} \right)^2 \quad (4)$$

With regards to transmission, transmittance values are typically only reported for the wavelength range of interest (e.g., usually visible light transmission only).^[52] For reference, **Table 1** provides the transmittance of some selected solid materials for the visible and near-infrared regions.

2. AR Coatings

AR coatings can be either used aesthetically (e.g., from reducing reflections on windows in a city^[19] to camouflage for insects^[6]) or functionally (e.g., from improving transmission through a moth's eye^[53] to reducing glare on screens, picture frames, and displays^[54]).

AR coatings were first identified in the 19th century when John Strutt (Lord Rayleigh) observed that transmittance increased in a tarnished piece of glass, contrary to his expectation. In trying to understand the physics behind this observation, Lord Rayleigh eventually reasoned that an AR coating was possible by gradually changing the refractive index as light passes through it.^[55] In later work by Bauer in 1934, the idea of engineering a dielectric coating to decrease the reflectance was proposed.^[11,56] Since these first few works, numerous successful AR coatings have been developed, most of which can be categorized into two main groups: layer-based and nanostructure-based coatings.^[57] Layer-based techniques can be considered “first generation” AR coatings and nanostructure-based coatings can be considered “second generation” AR coatings.^[53]

2.1. First Generation AR Coatings

The first generation of AR coatings utilizes abrupt changes in the refractive indices between layers, the substrate, and the medium on either side of the system to intentionally create destructive interference.^[53] In this way, the reflected wave is canceled out, achieving a situation where no reflection can emerge from the surface.

This happens when the incident light and the reflected light are exactly out of phase, as was first described in detail by Fabry and Perot.^[58] In nature, many examples of wave interference can be found, although examples of constructive interference (e.g., superposition of water and sound waves) are more readily noticed than destructive interference.^[59]

The equations and the details involved in calculating destructive interference for a single-layer film can be found in texts, such as by Macleod.^[11] For a single-layer coating, it turns out that the optical thickness of the coating should be one-quarter

Table 1. Transmittance of selected transparent solids.

Material	Thickness	Fabrication technique	(Average) Transmittance [%] (maximum)	Wavelength range [nm] (maximum)	Reference
Plate glass/plain glass/clear glass	N/A	Medium temperature melting/ forming	85–90	Visible spectrum	[233]
Natural diamond	1 cm	Natural heat/pressure event	≈68.5 (including Fresnel's reflection losses)	587.6	[12]
Polystyrene (PS)	N/A	Catalyst-assisted thermochemical reaction at 550–620 °C	88–92	Visible spectrum	[233]
Fused silica and quartz	1 mm	High-temperature crystal forming from a pure material melt	86–94	100–3000	[12]
Poly(methyl methacrylate) (PMMA) (organic glass)	N/A	Mass polymerization	<92	Visible spectrum	[233]
Float and drawn borosilicate glass sheet	25–3 mm	High temperature forming from a pure material melt	Min 67–88	Visible spectrum	[42]
Disks made of magnesium fluoride (single crystal)	2.7 mm	Precipitation/deposition followed by calcination	Minimum transmission > 90 (depends on surface orientation)	400–800	[232]
Tin oxide (TO) Carrier concentration: $9 \times 10^{18} \text{ cm}^{-3}$	600 nm	Chemical vapor deposition (CVD)	90–95	300–700	[48]
Antimony tin oxide (ATO) Carrier concentration: $1.2 \times 10^{20} \text{ cm}^{-3}$	360 nm	CVD	80–91	400–700	[48]
Indium oxide (IO) Carrier concentration: $4.7 \times 10^{20} \text{ cm}^{-3}$	270 nm	Evaporation	>90	300–700	[48]
Indium tin oxide (ITO) Carrier concentration: $\approx 10^{21} \text{ cm}^{-3}$	80 nm	Magnetron sputtering	>90	400–700	[48]
Zinc oxide (ZO) Carrier concentration: $\approx 2 \times 10^{20} \text{ cm}^{-3}$	100 nm	Magnetron sputtering	>90	400–800	[48]
Chromium titanium oxide (CTO) Carrier concentration: $2 \times 10^{21} \text{ cm}^{-3}$	≈1000 nm	Radio frequency sputtering	85	500–650	[48]
Two side-coated glass with monomeric liquid crystals	≈400 nm	Photoaligning	>96 integral transmission over the region: 99.1	400–700	[234]
Two side-coated glass with bilayers of SiO ₂ and TiO ₂ nanoparticles after calcination	Varied (to make quarter wavelength)	Layer-by-layer deposition	>96 (≈99)	400–800 (500–600)	[235]
Glass coated with a monolayer of SiO ₂	200 nm	Dip coating	>95	550–700	[236]
Glass coated with silica and poly- styrene nanoparticles	25 bilayers (20 + 60 nm)	Assembling an organic– inorganic nanocomposite	90–95	400–800	[237]
Glass coated with moth-eye patterned methacryloxypropyl terminated polydimethylsiloxane (M-PDMS) resin	≈325 nm	Hot embossing and UV nanoimprint lithography	94.8	400–800	[238]

of the wavelength of interest, $\lambda/4$.^[11] Thus, the optimal thickness of the single-layer AR coating, d , for normal incident light can be calculated by^[60,61]

$$d = \frac{\lambda}{4n} \quad (5)$$

Figure 4a shows a schematic of the way in which light interference occurs for a single-layer AR coating.

For the ease of calculation, normal incidence light is assumed, but incidence angle can certainly influence the design of AR coatings. To obtain $R = 0$ in the absence of absorption in an ideal single-layer AR coating at a particular

wavelength, normal incidence, and with air as the medium, leads to^[11]

$$n_{\text{film}} = \sqrt{n_{\text{air}} n_{\text{sub}}} \quad (6)$$

where the n_{sub} , n_{film} , and n_{air} are the refractive indices of the substrate, the AR coating, and the medium (air), respectively.

2.1.1. Multilayer AR Coatings

As can be seen in Figure 4b,c, a single layer does not provide broadband antireflectivity. In fact, it will give much higher

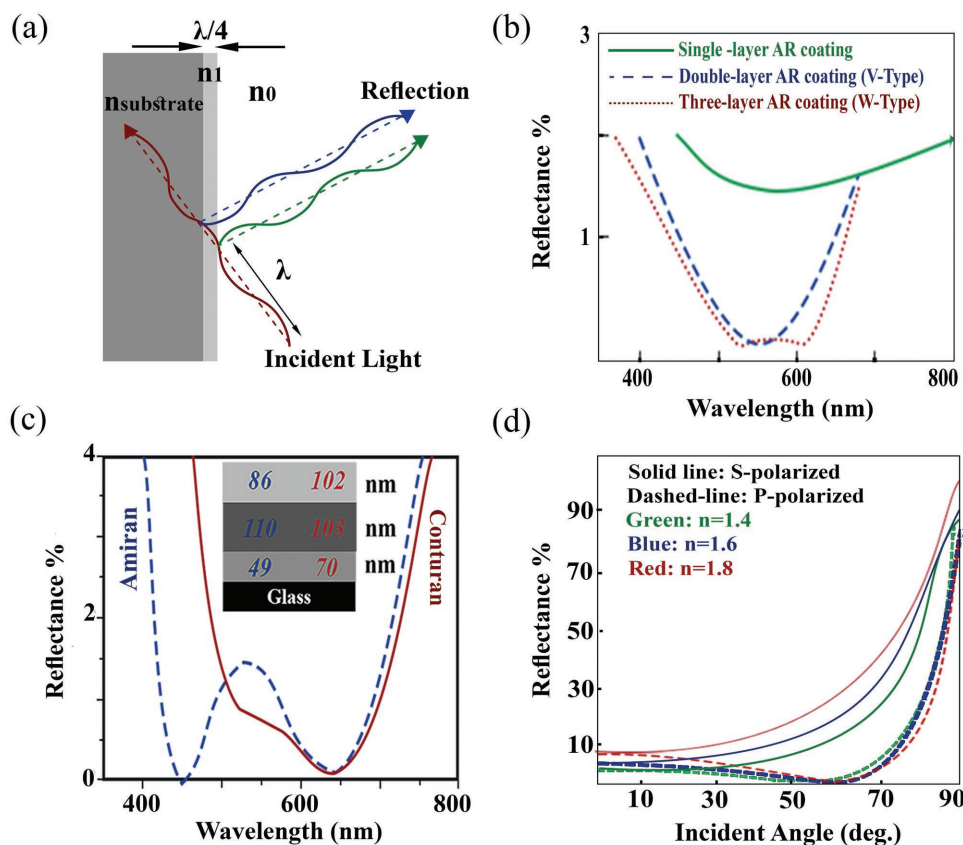


Figure 4. a) Destructive light interference in a single-layer AR coating. b) The general shape of optical spectra of coatings with a different number of layers (numbers are nominal). c) Amiran (blue dashed line) and Conturan (red line) AR glass. Reproduced with permission.^[60] Copyright 2012, Elsevier. d) Variation of reflectance with the angle of incidence for various values of refractive index.

reflection away from the design wavelength. Aside from the special case of laser applications, most materials interact with polychromatic light. Thus, broadband optical coatings are needed.^[11,54,62]

To improve upon the limitations of single-layer systems, multiple layer coatings can be employed. In fact, most natural examples of antireflectivity and selective reflectivity rely upon multilayer surfaces. Tiger beetles, *Cicindela*, for example, have a multilayer reflector in the outermost 2 μm of their integument which uses light interference.^[63] Another example is the outer scales of the East African sunset moth, *Chrysiridia croesus*, which also has a curved multilayer interference system of chitin/air (e.g., high and low refractive index pairs), to create iridescent wings.^[64]

For multilayer systems, an equation similar to Equation (5) can be written for paired layers of an AR coating with quarter-wavelength thicknesses. In a typical design, the layer closest to the substrate has larger refractive index than the substrate, while the outer layer has a smaller refractive index than the substrate.^[11,54]

$$\frac{n_{\text{low}}^2}{n_{\text{high}}^2} = \frac{n_{\text{air}}}{n_{\text{substrate}}} \quad (7)$$

With regards to a three-layer coating, the “quarter-half-quarter wavelength” AR design has been shown to provide good

broadband antireflectivity. These coatings are typically designed around two wavelengths of the interest, which yields a W-shaped curve, as is shown in Figure 4b. During deposition, a quarter-wavelength thick layer of the middling refractive index material is first applied to the substrate, followed by a half-wavelength, high refractive index layer, and finally a quarter-wavelength low refractive index outermost layer.^[60,62] Cox et al. designed a three-layer AR coating for the visible and near-infrared regions made of $\text{MgF}_2\text{-ZrO}_2\text{-CeF}_3$ on Crown glass. They posited that the thickness of the outer layer plays a prominent role in the antireflective effect, while small variations in the thickness of inner layers did not affect the antireflectivity of the coating.^[62]

It is noteworthy that there are also some more advanced multilayer designs, such as the four-layer AR coating designs by Sumita in 1973.^[65] However, advanced optics manufacturers rarely publish their designs, which are mostly based on trial and error.^[11] Thus, there are numerous proprietary commercial AR coatings, such as Conturan (commonly used in displays) and Amiran (which is frequently applied to architectural glazing – see Figure 4c).^[19]

2.1.2. Design Considerations

Material Considerations: The performance of AR coatings depends mostly on how well the refractive index of the

outermost layer matches with its surroundings (typically air). Unfortunately, there are no solid, transparent crystalline materials with low enough refractive indices to match air. MgF_2 ($n = 1.38$ at 500 nm), CaF_2 ($n = 1.44$ at 500 nm), and SiO_2 ($n = 1.46$ at 500 nm) are typically chosen as the lowest available refractive index materials.^[11,12,66,67] CaF_2 and MgF_2 have good refractive indices, but marginal mechanical properties.^[11,67] MgF_2 has the lowest refractive index, so it is often used for the outermost layer,^[11] but it should be deposited on a heated substrate for durability. As an alternative, SiO_2 might be the next best choice as it is tougher, lower in cost, and more stable, although it has a higher refractive index.

Comparing the Optical Performance of AR Coatings: Assuming the materials are proven to be stable and durable for their application, they can then be compared based on optical performance. The performance of AR coatings can be measured via spectral, diffuse, and/or total reflectance. Comparing specular AR coatings designed for a monochromatic light at a given incident angle is relatively straightforward, but many applications require the AR coating to perform over a range of wavelengths and/or angles. For most applications, this comparison can be done through a weighted reflectance, such as the solar-weighted reflectance (SWR).^[68]

$$\text{SWR} = \frac{\int_{\lambda_1}^{\lambda_2} R(\lambda) N_{\text{photon}} d\lambda}{\int_{\lambda_1}^{\lambda_2} N_{\text{photon}} d\lambda} \quad (8)$$

where $R(\lambda)$ is typically the spectral reflectance of the AR coating a (typically measured at 8°) and N_{photon} is the number of photons per unit area per unit wavelength in the AM1.5 spectrum.^[68] An analogous integration can be calculated numerically for other radiation sources and from either measured data or simulations of the coatings. It should also be noted that reflection at other angles or total/diffuse reflection may provide a more meaningful measure of performance in the above equation. Thus, a low (application specific) weighted reflectance gives a good measure of how well an AR coating fits its purpose. Thus, a standard specular reflection measurement alone is not usually enough to rank AR coatings. Absorption, scattering, and shifts in the transmission spectrum can all significantly change as a function of incident angle (in addition to other issues that might impair performance).

Effect of Incident Angle: Although many research papers have been published on the development of AR coatings, only a few (<50 since 1999, according to a 2017 Google Scholar search) have studied the effect of incident angle on the performance of AR coatings. Thus, although multilayer coatings are designed to decrease the reflection, they can actually increase the reflected light outside their design windows (e.g., at different incident angles, wavelengths, and polarizations).^[55] This makes designing a broadband and omnidirectional AR coating very arduous.^[69] For example, Thelen reported a design that for incident angles $< 20^\circ$, reflectance changes were insignificant. However, above 20° , rapid changes in reflectance were observed.^[70]

To complicate matters, polarized light interacts differently at different incident angles. S-polarized light has a reflectance curve that smoothly increases as a function of incidence angle. P-polarized light has a reflectance curve which initially decreases, but then increases rapidly after a minimum

(Brewster's angle) is reached.^[11] Typical reflection curves as a function incidence angle are plotted for polarized light and for visible wavelengths for a few refractive indices in Figure 4d.

Some researchers have been searching for the "ultimate" AR coating by devising algorithms to optimize the number of layers over a wide range of wavelengths (broadband) and incident angles.^[71–73] While there do not seem to be any natural laws that prevent this from happening (at least to some extent), many of the resulting designs would be nearly impossible to fabricate. For example, Liou and Liu proposed an algorithm to design an AR coating for the visible region and for different angles of incidence, up to 30° from normal. They used only three materials, ZnS ($n = 2.35$), Y_2O_3 ($n = 1.8$), and MgF_2 ($n = 1.38$), but were able to find designs that could decrease the reflectance to lower than 0.49% with 16–21 layers. Unfortunately, the thickness of some of the layers was specified to be just a few nanometers with very little tolerance, which would be really hard to uniformly deposit.^[71]

AR Coating Design Using Software: Multilayer films are cumbersome to design from the basic equations,^[11] so many modern tools have been developed for rapid optical simulations. Computational tools can use clever optimization routines and even some shortcuts, such as effective medium theory, in the analysis of AR coatings.^[53,74] OpenFilters,^[75] The Essential Macleod, Virtual Lab Fusion, FreeSnell, Software Spectra, and OptiLayer Thin Film Software are just some of the packages available for this purpose.^[76] OpenFilters is frequently used since it is a free, open-source software which can be used for designing AR coatings, calculating reflection, transmission, and optimization using needle, step, and Fourier transform methods. Additionally, as an open-source software, OpenFilters can be modified by the users according to their needs.^[75]

The main inputs for all of these software packages are the refractive indices and extinction coefficients, along with the reference wavelength(s) at which one intends to minimize the reflectance. Other inputs are the materials and their range of thicknesses for fabrication. For most materials, there are some useful databases available for optical constants.^[12,77] For uncommon materials, however, users may need to add their own materials by inputting their own refractive indices and extinction coefficients. The optical constants of materials, such as doped semiconductors, can be measured directly or calculated separately with known factors including free carrier concentration, temperature, structure, and other fabrication parameters (in addition to spectrum)^[77,78] (note: if it is important for the application, it may be necessary to determine (and thereby factor in) polarization dependence, as can be the case with TiO_2 ^[77]).

2.1.3. Gradient Refractive Index (GRIN) Coatings

Many transparent biological surfaces are GRIN materials. GRIN eye lenses can be found in humans, cows, lions, and several aquatic creatures – squids, octopus, some fish, and jellyfish (see Figure 5a,b).^[79] GRIN lenses consist of many thousands of (non-planar) layers made of proteins with gradually decreasing refractive indices (from the inner surface to the outer surface).^[80]

In the lab, depending on their fabrication, GRIN coatings can be considered as either the first generation AR coatings (if they

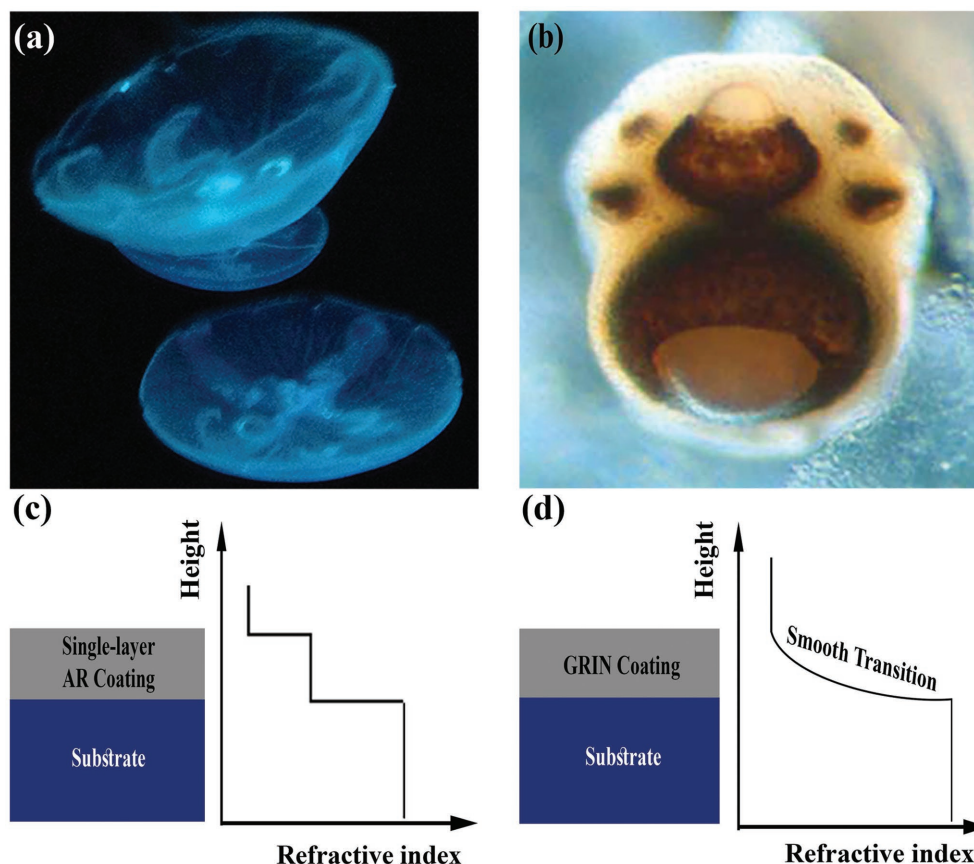


Figure 5. a) Jellyfish in an aquarium. b) The eyes of the box jellyfish, *Tripedalia cystophora* – have a gradient refractive index with a central refractive index of 1.48. The upper eye shows a smooth gradual decrease in the refractive index. In the lower eye, the core is almost homogenous surrounded by a smooth gradient. Reproduced with permission.^[39] Copyright 2005, Springer Nature. c,d) An ordinary AR coating versus gradual change in the refractive index of a GRIN coating.

consist of multiple layers) or the second generation of AR coatings (if they are patterned, as will be discussed in the next section).

As mentioned above, most multilayer depositions have trouble meeting the needs of applications which require broadband and omnidirectional AR surfaces (e.g., solar applications), but GRIN coatings have a chance to overcome some of these limitations. As inhomogeneous films in which the refractive index changes gradually in the z -direction^[74] (see Figure 5c,d), light is slowly refracted (e.g., bent with little reflection) as it moves through the GRIN, enabling more light to be transmitted through the system.^[74,81] Different profiles for the optimal variation in the refractive index as a function of the z -direction have been studied over the years. As provided by Southwell,^[82] common profiles are as follows

$$\text{Linear: } n = n_0 + (n_{\text{sub}} - n_0)t \quad 0 \leq t \leq 1 \quad (9)$$

$$\text{Cubic: } n = n_0 + (n_{\text{sub}} - n_0) \times (3t^2 - 2t^3) \quad (10)$$

$$\text{Quintic: } n = n_0 + (n_{\text{sub}} - n_0) \times (10t^3 - 15t^4 + 6t^5) \quad (11)$$

where n_0 , n_{sub} , and t are the refractive index of the incident medium, the refractive index of the substrate, and the thickness

(Southwell assumed the graded interface region to be 1 μm thick) of the GRIN structure, respectively.^[82]

GRIN coatings can be fabricated with physical vapor deposition (PVD), etching, and glancing angle deposition (GLAD), or other advanced techniques, but first generation GRIN structures are relatively complicated (and expensive) to produce.^[83] As an example, Bartzsch et al. deposited a GRIN coating made of a ternary compound of $\text{Si}_x\text{N}_y\text{O}_z$ by reactive pulse magnetron sputtering. The reflectance across the range of 440–620 nm was reported to be less than 0.5% for their device.^[84] Senda et al. made a thin film of fluoropolymer using ion-assisted vapor deposition polymerization to obtain a GRIN coating with good adhesion and low surface energy.^[85] Wang et al. developed a GRIN of indium tin oxide (ITO) to improve the performance of a V-pit light-emitting diodes.^[86]

2.2. Second Generation AR Coatings

As discussed above, layer-based AR coatings have several limitations: material selection (nonideal refractive indices, $\text{MgF}_2 = 1.38$ being the lowest), fabrication costs (due to complicated depositions), angular and spectral dependence. To overcome these, researchers have had to look to nature for

help. Through this, the second generation of AR coatings has emerged which relies on porous coatings and/or subwavelength structures (SWSs).

2.2.1. Porous AR Coatings

Taking the nominal case of air as the incidence medium ($n = 1$) and window glass ($n = 1.51$) as the substrate, the root mean square of these two would indicate that the ideal single-layer coating should have a refractive index of 1.23 (recall: Equation (6)). Since there are no solid materials with such a low refractive index, new materials have been under development. Porous materials represent a promising approach. Raut et al. reported a porous polymer-based MgF_2 AR coating with refractive index of almost 1.23, for the spectrum between 600 and 800 nm.^[87] Remarkably, researchers have developed materials with even lower refractive indices – e.g., ≈ 1.09 for porous MgF_2 , ≈ 1.05 for SiO_2 nanorods and porous poly(methyl methacrylate) (PMMA), ≈ 1.04 for CaF_2 nanograss, and ≈ 1.03 for low-density carbon nanotube array,^[88] and, aerogel which can be as low as 1.01.^[89] These pores should be smaller than 80 nm to avoid scattering of visible light. This pore size is referred to as the “nonscattering porosity.” If the pores are larger, the coatings will start to take on a diffuse white appearance, which indicates scattering losses.^[54]

Predicting, the refractive index of these materials relies on either empirical relations or effective medium approximations. As an example, the following effective medium equation provides a relationship between porosity and refractive index from Yoldas and Partlow (pore size < wavelength)^[90] which seems to match well with experimental data

$$n_p^2 = (n_d^2 - 1) \cdot (1 - P) + 1 \quad (12)$$

where n_p , n_d , and P are the refractive index of the porous material, the refractive index of the dense material, and the volume fraction ($0 < P < 1$) of nonscattering porosity, respectively.^[90] It can also be rewritten in a way that P is in percentage (i.e., $0 < P < 100$).^[53] As pointed out by Braun and Pilon,^[91] these types of equations should be used with care, however, because they are only valid above a critical nanoporous film thickness. Below this critical thickness, other factors including pore size, shape, and spatial distribution begin to dominate the refractive index of the porous structure.^[91]

Another example is Lorentz–Lorenz classical equation, also called as Clausius–Mossotti,^[92] which gives the relationship between the material composition and the refractive indices in a multicomponent system.^[93]

$$\frac{n^2 - 1}{n^2 + 2} = \sum V_i \frac{n_i^2 - 1}{n_i^2 + 2} \quad (13)$$

in which V_i , n_i , and n are the volume fraction of component i , the refractive index of component i , and the refractive index of the system, respectively. In this model, air is thought of as a solid component with $n_{\text{air}} \approx 1$. By summing up, the effective refractive index of a porous film can be found, although it should be noted that this equation can be only used safely when the porosity is high enough ($P \geq 0.7$).^[92]

2.2.2. Material Selection for Porous AR Coatings

Porosity can be introduced via numerous routes,^[54] with the wavelength range of low refractive index and mechanical durability being the two biggest considerations. As was pointed out by Yoldas and Partlow, SiO_2 , Al_2O_3 , La_2O_3 , ThO_2 , and HfO are all potential materials for the UV region, but due to high refractive indices (except for SiO_2), a porosity of higher than 80% would be needed.^[90] It seems that among inorganic oxides and fluorides, MgF_2 ,^[87,94] SiO_2 , CaF_2 ,^[67] TiO_2 ,^[61] and Al_2O_3 ^[60,95] are still some of the only practical materials of interest for porous AR coatings. Of these, TiO_2 might be one of the most attractive materials for future work due to its potential as a hydrophobic/hydrophilic (self-cleaning) surface, which will be discussed later.

2.2.3. SWS AR Coating

Another category of AR coatings relies on the “moth-eye” structure – a concept for which our understanding dates back 1960s when Bernhard and Miller found identical cone-shaped protuberances on moth’s eyes under an electron microscope.^[96]

In a moth’s eye (Figure 6a,b), these patterned surfaces are made of chitin (a polysaccharide with $n \approx 1.54$), and due to that, their GRIN structure can decrease the reflection by nearly a factor of 10.^[6] Bernhard et al. studied 361 species of different insects, categorizing them based on micro-/nanostructure size into three different groups – i) insects with structures less 50 nm in height, ii) insects with 50–200 nm high structures, and iii) insects with structures higher than 200 nm. They tried to confirm the antireflectivity of the structures through scaling them up in diameter, height, and wavelengths. They made artificial nipple-shaped structures out of paraffin and beeswax (3:1), with a solid refractive index of 1.5^[64] (very near the real material, which has $n \approx 1.54$ ^[6]). They observed some improvement in the transmission and a drop in reflection over a wide wavelength using their design.^[97] Years later, Clapham and Hutley conclusively showed how the moth’s eye works by analyzing the effect of the wavelength and the structure size.^[98,99] If the structure is bigger or equal to the wavelength, the structures act similar to any other surfaces at the macroscale. On the other hand, if the structure is much smaller than the wavelength ($\lambda \gg h$) (see Figure 6c), the structure will not act as a GRIN coating. Therefore, the structure needs to have a height above, but not too much greater than, a critical ratio of $h/\lambda \approx 0.4$.^[98,99]

The moth’s-eye structure has been mimicked with many materials/techniques in the lab.^[53,74,100,101] A nanopillar design, reported by Ji et al., indicated a trade-off between reflectance and scattering with respect to the height of the pillar (e.g., scattering becomes dominant for tall pillars).^[102] This limits the effectiveness of this type of GRIN, but for the visible region, it is clear that h should be ≥ 250 nm.^[98] Another important factor in the design is the periodicity, Λ , which should be small enough to avoid diffraction. Unfortunately, this depends on the incident angle. Thus, a design for normal incident light would have a smaller periodicity than one designed for 60°. Another issue is that while reflection may well be reduced in

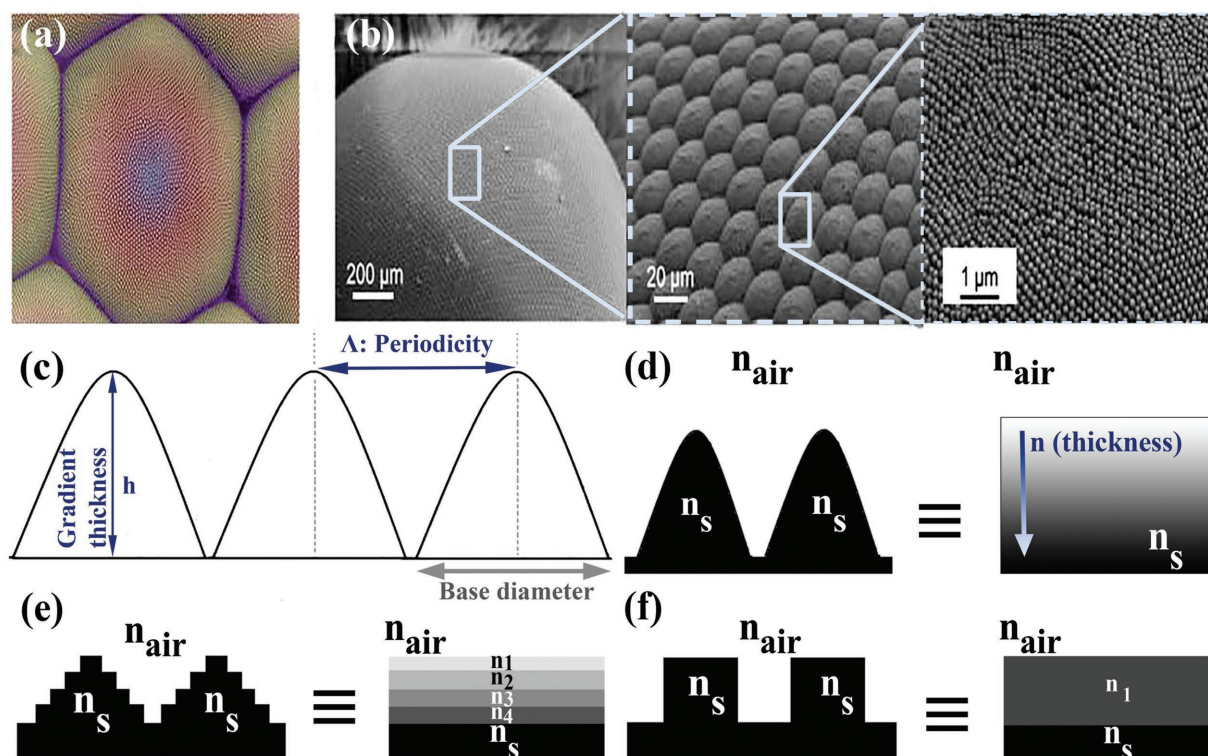


Figure 6. a) A scanning electron microscope (SEM) image showing tiny bumps on moth's eye. b) Increasingly magnified SEM images showing the hexagonal array of SW nanostructures. Reproduced with permission.^[53] Copyright 2011, Royal Society of Chemistry. c) Simplified schematic picture of the moth's-eye structure. d) Schematic profile of SWSs with a moth-eye GRIN structure (nanococones), e) multilayer SWS AR coating with a stepped profile, f) SWS nanorods which act as a single-layer AR coating (modified from ref. [226]).

these structures, it can arise from light trapping in the SWSs due to multiple internal reflections. This is a major issue with SWS that “first generation” AR coatings do not face. Thus, to ensure transmission through the structure, the periodicity should be even smaller – e.g., $\Lambda < \lambda/n$, which enables light to pass through the SWSs. For oblique angles of incidence, the scale may need to reduce even further, to say $\Lambda < 0.5\lambda/n$, to maximize transmittance.^[99]

Several studies have agreed that SWSs with higher aspect ratios and properly chosen periodicity to perform best.^[69,103] Even this is not the full story since the shapes used in SWSs can also alter performance. Some shapes act as single-layer AR coatings (e.g., nanorods), while others behave like multilayer AR coatings (e.g., triangular, conical, parabolic, truncated cone, etc.)^[104] (see Figure 6d–f). Some researchers use effective medium approximation approaches to model these nanostructures, but since the wavelength of the light has the same scale as the structure, it becomes necessary to solve Maxwell equations directly to avoid any inaccuracies such as overestimation in reflectance, for instance.^[105] Modeling these structures can be done numerically. For example, rigorous coupled-wave analysis (RCWA) is one of the numerical methods which are used by researchers to model periodic optical structures.^[106] There are some commercial software packages on the market, such as UNIGIT,^[107] which use RCWA. There is also free software to solve Maxwell's equations, such as a MATLAB-based finite-difference frequency-domain (FDFD) method developed by Shin.^[108]

The final key issue of the moth's-eye design is durability/reliability. Although adult moths have relatively short life spans (a week or two^[109]), their natural nanostructured eyes enjoy exceptional durability/reliability, if you stop to consider their operational environment. At present, most nanotechnology researchers work in either clean rooms or cleanrooms and avoid exposing their synthetic materials to degradation and fouling from temperature, moisture, and dust/dirt.

2.2.4. Hybrid AR Coatings

Many porous “hybrid” thin films (mixtures of first and second generation AR coatings) have been made, based on polymers and inorganic oxides or fluorides. The main aim of “hybrid” designs is to decrease the reflection while increasing the transmission (e.g., to get the best features from both).

One possibility is using porous materials in a multilayer system with a quarter-wavelength structure.^[90] For instance, Li et al. reported a broadband and omnidirectional AR coating based on a polystyrene-*block*-poly(methyl methacrylate) (PS-*b*-PMMA)/PMMA blend onto an octadecyl trichlorosilane (OTS)-coated substrate.^[110] However, it was found that having a quarter-wavelength coating of an ordinary porous film is not sufficient to achieve a broadband and omnidirectional AR coating. Therefore, it has been recommended that these porous structures should be coupled with GRIN coatings to get closer to an ideal AR coating.^[90]

Cui et al. reported an MgF_2 - SiO_2 hybrid, trilayer, porous AR coating. This yields a multilayer porous coating which represents a mixture of both first and second generation AR coatings. The transmittance was almost 99% throughout the studied wavelength range (350–1100 nm).^[111] Khan et al. reported another three-layer hybrid design which sandwiched a dense layer, a spongy layer, and a porous structure, respectively, adjacent to a substrate made of HfO_2 through a glancing angle deposition technique. They used fluorine doped tin oxide (FTO) and sapphire as their substrates and were able to decrease the reflectance to less than 1% in the visible region.^[112]

Another possibility is using SWSs in a multilayer system. Bruynooghe et al. reported a hybrid design wherein the outermost layer was designed to have the smallest refractive index (e.g., moth-eye structures), while the inner layers were a more traditional multilayer AR coating. They observed that their AR coating had a very low reflectance, across the 250–850 nm range. The residual reflectance at 20°, 40°, and 60° of incident angles were 0.5%, 0.77%, and 2.69%, respectively.^[66]

In another study by Schulz et al., a dense silica layer and melamine SWSs were deposited via plasma ion-assisted deposition before etching. The resulting hybrid AR coating was capped with silica, which enabled an antireflectance over the wavelength range of 400–800 nm for 0°, 45°, 60°, at about 1% reflectance on average.^[113]

Perl et al. came up with a design on sapphire and gallium nitride as substrates to decrease the reflectance to 0.2% and 0.6%, respectively (for 300–1800 nm). Their design consisted of multilayer AR coating made of Ta_2O_5 and SiO_2 (i.e., a first generation AR coating) and the outer layer was SiO_2 nanostructures.^[114]

3. AR Materials and Fabrication Techniques

The materials chosen for AR coating fabrication are very much dependent on the substrate – glass, plastic, or biological substrates are used. In the case of plastic and biological substrates, processing usually has temperature limitations.^[115] Additionally, the thermophysical properties of the AR coatings should match with those of the substrate.^[116] Thermal mismatch between materials and the substrate can cause delamination – a key reliability issue for AR coatings.^[117] Along these lines, it has been found that metal oxides are very difficult to deposit on polymeric substrates because of their different thermal expansion coefficients which cause stress and eventual delamination. The thermal expansion coefficients of polycarbonate and SiO_2 are 65×10^{-6} and $0.5 \times 10^{-6} \text{ K}^{-1}$, a factor of 130× different. Sputtering is also not suitable for plastic substrates on the account of radiolytic damage to polymer chains.^[118] This may justify the development of more techniques to develop AR coatings for plastic substrates, but polymers do not have as much variety in their refractive indices as metal oxides.^[118] SWSs (on glass substrates) have been found to suffer less from thermal mismatch issues. This is increasingly important for laser applications since they can push toward higher laser-induced damage thresholds.^[24]

3.1. Material Selection

To select AR materials, it is essential to know the optical constants (n and k across the spectral region of interest),^[11] the resistivity, electrical conductivity, the chemical durability (e.g., durability at different pH and humidity values), the thermal stability, and potentially, the toxicity of the AR materials. Although the optical properties may be acceptable, these other factors may disqualify many materials for most applications.^[119] An overview of the range of materials, substrates, and applications for AR coatings is shown in Table 2. To address this complex issue, Gordon came up with an equally elaborate selection criteria for choosing transparent conductors to determine the best-fit materials for the application,^[29] which should be reviewed by the interested reader.

3.2. Fabrication Techniques

As can be seen in Figure 7a, there is also a wide range of different fabrication techniques to choose from – each of which has benefits and limitations.^[11] Natural biological materials, of course, usually repair and replace themselves over time – and, importantly, do so at low-temperature with non-toxic materials. Low-temperature synthesis methods are not common for the materials shown in Table 2. For example, the cuticle of most insects contains chitin, a biopolymer made of N -acetyl- β -D-glucosamine and structural proteins (sclerotized proteins). Since chitin makes the cuticle rigid, the growth and development of the insect are contingent upon replacing its cuticle throughout its life span.^[120] In the lab, deposition and nanotexturing methods have advanced a lot in recent years. Nanotexturing can broadly be categorized into three groups – microreplication process (MPR) (i.e., nanoimprinting or injection nanomolding), metallic mold electroplating (i.e., roll-to-roll manufacturing), and replication into plastics (i.e., using templates like anodic aluminum to generate a porous aluminum membrane).^[121]

Like many materials, second generation AR coatings can be made either through bottom-up or top-down techniques. Top-down methods remove material from a substrate and include dry and wet etching (see the examples in Figure 7b–e). As one example, some of the moth's eye-inspired AR coatings have been made through reactive ion etching (RIE). The difficult part of this is getting a 3D structure from a 2D technique. One solution to this is to utilize self-assembled colloidal lithography (e.g., polystyrene nanosphere) or a thin layer of metal (e.g., Al, Au, Ag, etc.) as the etching mask. This technique has recently advanced to include block copolymer micelle lithography (BCML), which enables tunability/organization of the spacing between metallic nanoparticles to yield greater control over the AR SWSs made with RIE.^[122,123]

Bottom-up methods, on the other hand, involve depositing coatings onto a substrate. Common bottom-up techniques include sol-gel methods, chemical vapor deposition (CVD) techniques like plasma-enhanced CVD (PECVD), PVD, and GLAD. There are also a few “other” methods, which do not neatly fit into either additive or subtractive manufacturing categories, with some examples mentioned

Table 2. Selected overview of the materials used for AR coatings.

Material	Substrate	Application	Reference
CeO ₂ /MgF ₂ and ZnS/Na ₃ AlF ₆	Glass	Visible region AR coating	[56]
MgF ₂	Ge	IR region AR coating	[56]
Ge and Si	Glass	Optical storage	[239]
MgF ₂ , SiO ₂ , SiO ₂ , Al ₂ O ₃ , CeF ₃ , ThO ₂ , Nd ₂ O ₃ , ZrO ₂ , CeO ₂ , and ZnS	Glass	AR windshield	[240]
MgF ₂ , SiO ₂ , Al ₂ O ₃ , Ta ₂ O ₅ , TiO ₂	Glass	AR coating for wide angular incidence	[72]
SiO ₂ , TiO ₂ , SnO ₂ , and ITO	PET foils	Multilayer AR coating	[241]
ZrO ₂ and Al ₂ O ₃	Poly(methyl methacrylate) (PMMA), polycarbonate (PC), and fused silica	AR coatings in the spectral range $\lambda = 800\text{--}900\text{ nm}$	[242]
SiO _x /TiN/SiO ₂	Plastic film	Cathode ray tubes (CRTs)	[243]
SiO ₂ and TiO ₂	Glass	Near-infrared AR filter	[244]
SiO ₂	Silica	Lenses, windows, blast shields, debris shields, and harmonic converters required for MJ-class laser	[245]
ZnSe, ZnS, Ge, YF ₃ , and YbF ₃	MgF ₂	Infrared AR and protective film	[116]
SiO ₂ , Al ₂ O ₃ , Ta ₂ O ₅ , Si ₃ N ₄	Polymer substrates	Multifunctional gradient coatings with antireflectivity and scratch resistance	[246]
Zeolite	Glass	Scratch-resistant AR coating for solar applications	[134]
TiO ₂ , TiN, TiAlN	Glass	Low-emissivity coatings	[247]
ZnSnO (ZTO) and Ag	Al ₂ O ₃ /150 nm thick crystalline ITO/glass substrate	AR coating for highly transparent ZTO channel-based thin film transistors (TFTs)	[248]
Silica nanoparticles and poly (diallyldi- methylammonium chloride) (PDMA)	Glass	Broadband AR coating for self-cleaning photovoltaic cells	[249]
Silica and polystyrene	Glass	Enhancing photovoltaics with broadband high transparency Glass	[250]
Nb ₂ O ₅ and SiO ₂	Glass	Hybrid broadband AR coatings with wide-angle properties	[66]
Fused silica (nanopillars)	Fused silica	Nanostructured stealth surfaces for visible and near-infrared light	[122]
SiO _x -AlN	Glass	High hardness and high transparency for touchscreens	[251]
GdF ₃ /MgF ₂	CaF ₂ substrates	AR narrow-band ultraviolet filter	[252]
CaF ₂	Borosilicate glass	AR coatings	[67]
Silica/polymer composite coatings	Glass and poly(methyl methacrylate) (PMMA)	Biomimetic AR coating	[253]

in Figure 7a. The interested reader can find several excellent, detailed reviews on the recent advances in AR fabrication in the literature.^[53,74,101,115,124,125]

In the review by Chen,^[115] several of the most common methods including sol-gel process, e-beam evaporation, and sputtering were compared on basis of materials, operation conditions, and cost. Chen reported that although all these processes are controllable, all the methods except sputtering are limited to a selected set of raw materials and both spin coating and e-beam evaporation were noted to be limited in scale. In the end, Chen suggested that dip coating is the best candidate to scale up for commercial AR coating production.^[115]

Many man-made AR coatings have surpassed the optical performance of their natural counterparts. However, natural materials still have several advantages in terms their multifunctionality and fabrication “costs,” as will be discussed in the next few sections. It should be noted that—as with an antireflective function—many of these functions would be advantageous if implemented into transparent materials.

4. AR Coatings in a Multifunctional World

Multifunctionality helps creatures adapt to their habitats and to hide from their predators/prey. Moths, butterflies,^[126] and cicadas^[127] all exhibit multifunctional surfaces. That is, by combining antireflectivity with self-cleaning, these creatures fly through life with little deterioration in their optical properties.

Although usually overlooked, many plants have surfaces which offer examples of multifunctionality (e.g., durability and self-cleaning during the simultaneous light and water management), which make them well-suited to their interaction with their environment.^[128] It is evident that dust and contamination will reduce light transmission, but when considering transparent materials, there are myriad functions which could be tacked on to improve overall performance, such as modified thermal conductivity (e.g., windows, glazings, and solar thermal covers),^[129] flexibility (e.g., in curved and flexible displays),^[130] antifogging,^[131] self-cleaning (i.e., (super)hydrophilicity/hydrophobicity^[132]), photocatalysis,^[133] mechanical/chemical

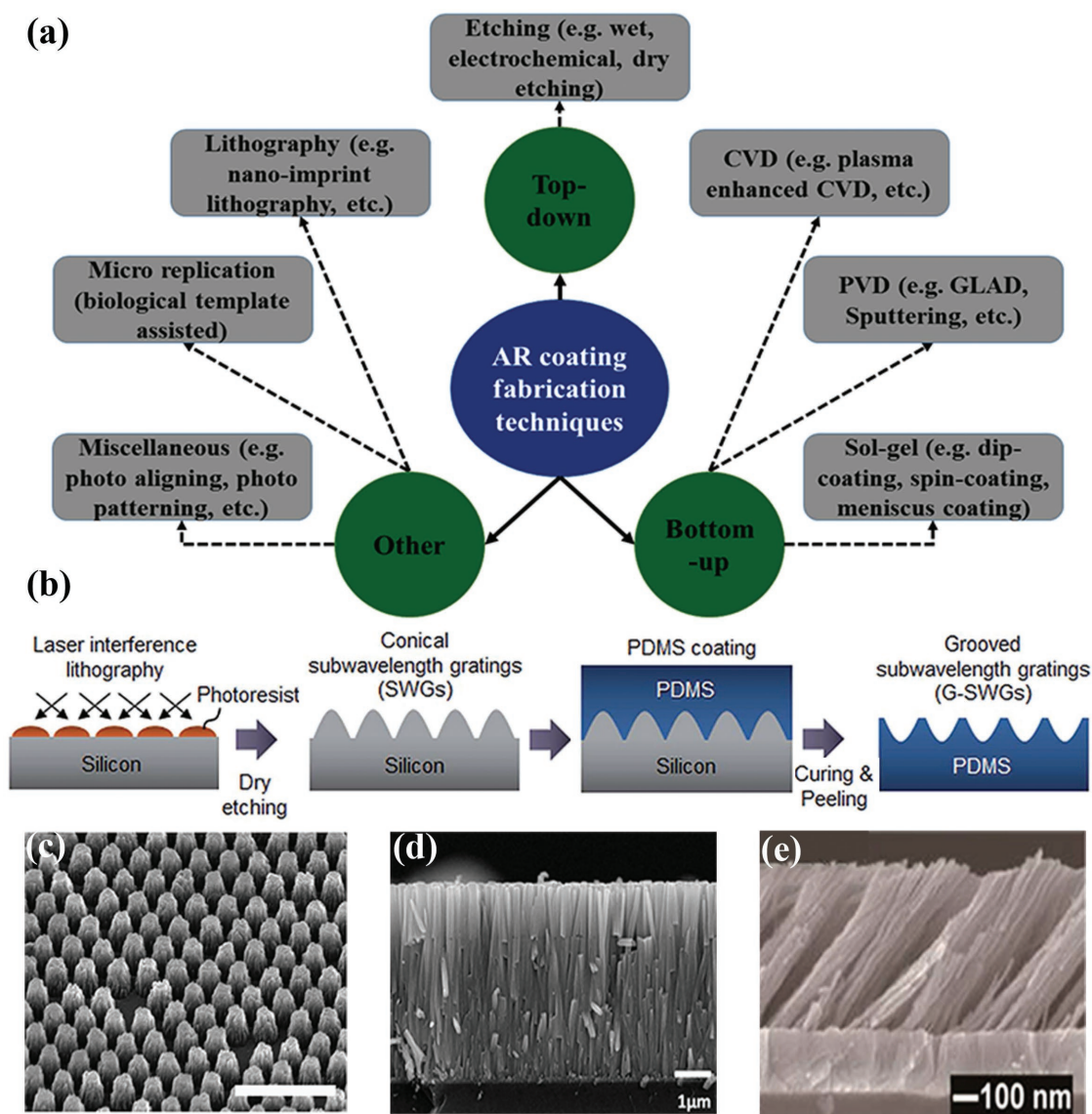


Figure 7. a) Common methods used to fabricate AR coatings. b) Fabrication steps for SW gratings on the surface of PDMS films using a conical silicon mold with soft imprint lithography method. Reproduced with permission.^[227] Copyright 2016, Royal Society Chemistry. c) SEM image of SWS on fused silica after 7 min RIE. Reproduced with permission.^[24] Copyright 2016, Elsevier. d) A cross-sectional view of ZnO nanorods made by atomic layer deposition. Reproduced with permission.^[228] Copyright 2018, Elsevier. e) SEM profile of WO₃ coated on glass using GLAD at 75°. Reproduced with permission.^[229] Copyright 2016, ACS Publications.

hardness (i.e., antiabrasion, antisoiling, and anticorrosion^[134]), electrical properties (such as conductivity^[135] and antistatic control^[136]). Other useful functions include biocompatibility (e.g., contact lenses),^[137] sensing (e.g., biomolecular sensing),^[138] and antimicrobial coatings.^[139] For transparent materials, these areas are sure to grow as multifunctionality becomes more technically and commercially feasible.

In the context of this review, self-cleaning surfaces can be considered as one of the lowest hanging fruits for transparent materials. Imagine adding an expensive AR coating to a product, only to have it literally and figuratively gather dust in the hands of the consumer. Well-designed self-cleaning (and easy cleaning) surfaces have a much longer service life and are easier to maintain in the unavoidable presence of contaminants, dust, moisture,

and oils. A shining example of this are coated photovoltaic modules C-Voltaics, a start-up energy company from the University of Houston which has licensed a "Self-Cleaning Hydrophobic Coatings (SCHN107TM) Layer," which have been tested to maintain solar transmission in the presence of dust and water for their full life.^[140] Another innovative instance of multifunctional transparent surfaces is the new type of "smart" windows, developed by the University College London researchers, which minimizes heat loss and the need for cleaning by using nano-structured vanadium oxide on glass.^[141]

Self-cleaning can be intriguing to integrate with antireflectivity not only for maintaining optical properties but also because the fabrication/preparation techniques have striking similarities—indicating the potential for clever shared synthesis methods.

Table 3. Natural multifunctional examples.

Species	Shape	Spectral properties	Self-cleaning type (contact angle)	Reference
Neck feathers of mallard drakes (<i>Anas platyrhynchos</i>)	Rods – hexagonal arrays Diameter ≈ 130 nm	Directional bandgaps in the green and UV regions	Superhydrophobic (152°)	[36]
Cicada wings	Pillars – arranged in a hexagonal array (inset) with 190 nm interpillar spacing.	For <i>Cryptympana atrata Fabricius</i> : reflectance = 2% (visible region), < 8% (visible region) for smooth wing (crushed protuberances)	Hydrophile/hydrophobe (76.8°–146°) (depending on the species) (for <i>Terpnosia jinpingensis</i> = 146°)	[74,173]
Butterfly wings	Scale: Distance: 48–91 μm Length: 65–150 μm Width: 35–70 μm Vertical gibbosities: Distance: on scale is 1.06–2.74 μm Height: 200–900 nm Width: 200–840 nm	Reflectance peak at the wavelength of wing's color for blue Morpho butterfly (460–500 nm) Minimum absorbtivity from 450 to 500 nm	(136.3°–156.6°) (depending on species)	[254,255]
Peacock feather	Rods – a barbule consists of a medullar core of ≈ 3 μm enclosed by a cortex layer Rod length ≈ 0.7 μm	Blue and green barbules: reflectance peaks with narrow widths blue and green light, respectively Yellow barbules: peak reflectance ranges from the green to the orange Brown barbules: peak reflectance from the green to the red wavelength	N/A	[256]

4.1. Wettability and Light Reflection/Transmission

A material's wettability, or lack thereof, is dictated by the physical chemistry of a relatively thin outer surface layer (≈ 1 μm) of a material. Since most of the energy of sunlight is also absorbed or reflected in that same 1 μm, this very thin outer layer of many natural materials manages both light and water. **Table 3** shows a summary of species which have been studied for their sophisticated photonic nanostructures and their self-cleaning attributes. While this seems like a natural union of properties, not much research is chasing this duality. Of the >3000 papers published by early 2018 with “antireflective” or “antireflection” in the article titles, only 2.3% also mention “cleaning,” “hydro,” or “wettability” (based on a January 2018 Scopus search). Thus, to date, man-made AR coatings and “self-cleaning” materials^[142] have developed largely in isolation, despite their strong potential for synergy. As just one motivating example, there are several studies on the mechanisms and impacts of soiling on the performance of solar energy technologies, as was summarized in a recent review by Mani and Pillai.^[143] Even for less demanding indoor applications, a highly engineered (read: potentially expensive) AR coating would greatly benefit from being resistant to water and dust, helping to maintain its optical properties over time. As will be discussed below, there are several viable ways to approach this goal since self-cleaning can be done through either a hydrophilic or a hydrophobic route.

4.1.1. Self-Cleaning Coatings

“Self-cleaning” can be derived from two opposing pathways – via either a hydrophilic or a hydrophobic surface. As perhaps the most widely known self-cleaning surface, the leaf

of the lotus plant, *Nelumbo nucifera* (**Figure 8a–d**) represents the epitome of the natural “superhydrophobic” (which will be described later) surface.^[144] On a hydrophobic self-cleaning surface, water beads up and slides and rolls-off these surfaces, removing dirt and contaminants as it goes; whereas, in the case of hydrophilic cleaning, water completely wets the surface to carry dirt and contaminants away. As an example of this, consider your eyes which regularly flush out dirt and debris. To distinguish between these two routes in the context of AR coatings, wettability of the coating should be checked by measuring the contact angle (CA), the angle θ which a droplet of water makes when in contact with the surface of the coating. This static contact angle on a smooth surface (without roughness) can be predicted by Young's equation.^[145] Thus, AR coatings can be also classified based on CA (see **Figure 8e,h**)^[146] (note that different ranges of CA for hydrophobic surfaces have been suggested).

$$\cos \theta = \frac{(\gamma_{SV} - \gamma_{SL})}{\gamma_{LV}} \quad (14)$$

where, γ_{SV} , γ_{SL} , and γ_{LV} are the interfacial tensions of the solid–vapor, solid–liquid, and liquid–vapor interfaces, respectively.

AR coatings can be considered as a hydrophobic surface, by definition, if water is nearly not adsorbed or weakly adsorbed by the coating, in other words, water does not spread on their surfaces. This adsorption can increase by a temperature rise. There are some models to relate CA to surface roughness in general which is worthwhile to be noted. Wenzel argued that in reality, the interface of the liquid and solid cannot be smooth because the real surface is not identical to

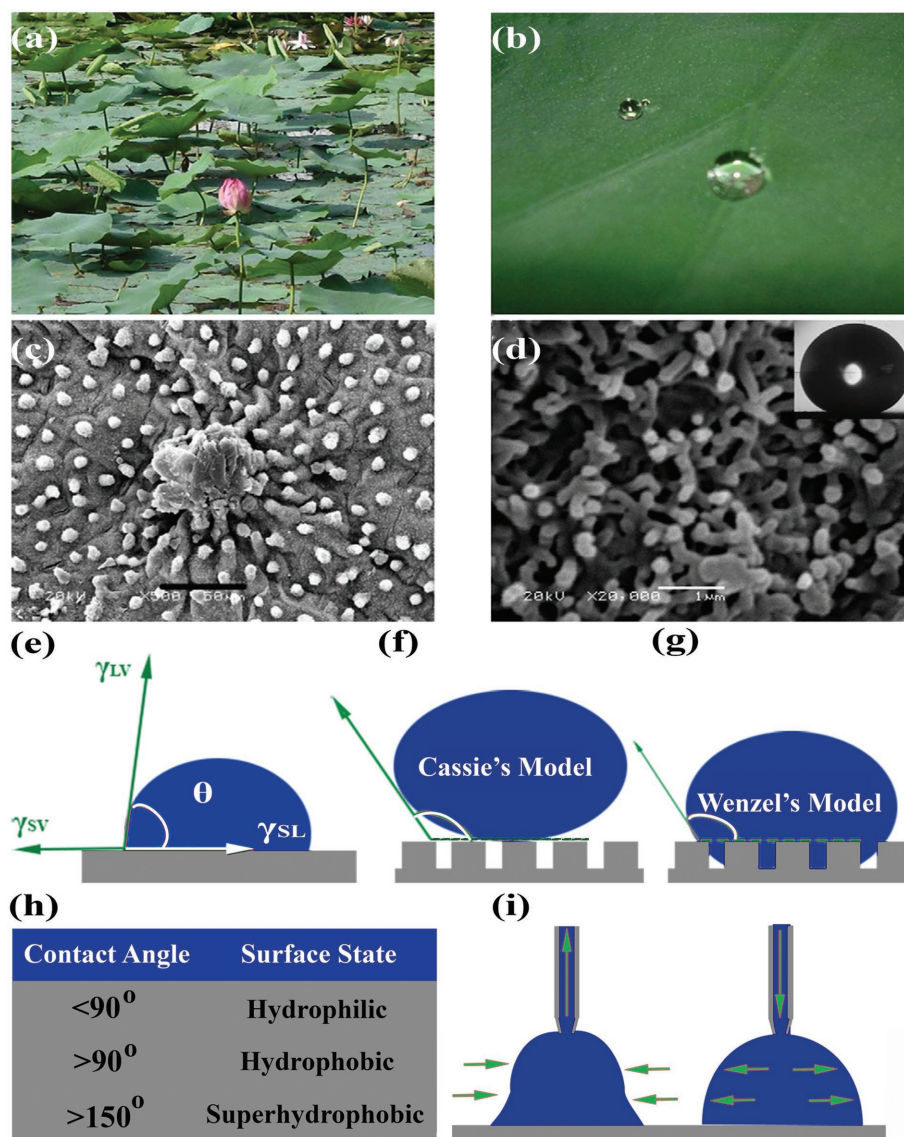


Figure 8. a) Lotus leaves on a pond. b) Droplet of water on a leaf. c) SEM image of a lotus leaf. d) Zoomed in SEM image of a lotus leaf with inset image of a droplet on the leaf having a contact angle of 161° . Reproduced with permission.^[34] Copyright 2007, Elsevier. e) Cartoon of a liquid droplet on a (smooth) surface. f) Cartoon of a liquid droplet in Cassie state. g) Cartoon of a liquid droplet in Wenzel state. h) Surface state classification based on static contact angle. i) Cartoons of receding (left) and advancing (right) contact angles.

the geometric surface (flat projected area). Wenzel defined a roughness factor, r ^[147]

$$r = \frac{\text{actual surface}}{\text{geometric surface}} \quad (15)$$

Based on Wenzel model (homogenous wetting regime – water penetrates completely into the surface roughness^[148]) proposed in 1936, the CA on a rough surface, θ_{rough} , is related to that of the smooth surface, θ_{smooth} .^[33]

$$\cos \theta_{\text{rough}} = r \cdot \cos \theta_{\text{smooth}} \quad (16)$$

Later on, Cassie and Baxter proposed another model based on which the droplet on a rough surface cannot penetrate

the surface cavity (Figure 8f). Instead, the droplet sits on the trapped air in the surface cavities (heterogeneous wetting regime^[148]). Therefore, CA in their model can be found using

$$\cos \theta_{\text{rough}} = f \cos \theta_{\text{smooth}} + f - 1 \quad (17)$$

where f ($0 < f \leq 1$) is the fraction of the projected area of solid (it is worth noting that Equations (16) and (17) are correct if the droplet size is larger than the roughness). Furthermore, there are some thermodynamics considerations/complexities (such as metastable configuration which are caused by the reversible transition between Wenzel and Cassie–Baxter state) to find out the state (Wenzel or Cassie and Baxter) of a droplet on a surface.^[149] In short, a water-repellent surface when it is rough repels water more than when it is smooth. By the same token,

Table 4. Natural superhydrophobic materials and their static CAs.

Species	Static contact angle	Reference
Lotus leaf	$161^\circ \pm 2^\circ$	[34]
Rice leaf	$157^\circ \pm 2^\circ$	[34]
Rose petals	152.4°	[171]
Fish scales	Oil contact angle $> 150^\circ$	[33]
Ramee leaf	Front surface: $38^\circ \pm 2^\circ$ Rear surface: $164^\circ \pm 2^\circ$	[34]
Taro leaf	$159^\circ \pm 2^\circ$	[34]
Chinese watermelon	$159^\circ \pm 2^\circ$	[34]
Mallard drake	152°	[36]
Cicada wing	76.8° – 146° (depending on the species)	[173]
Butterfly wings	136.3° – 156.6° (depending on the species)	[254]
Water strider	$167.6^\circ \pm 4.4^\circ$	[35]
Gecko (toe pad)	$\approx 150^\circ$	[257]

when the surface is hydrophilic, it will be more hydrophilic if it is rough.^[147]

Interestingly, in some cases, surfaces may appear to be waterproof, but this phenomenon can just be related to capillary forces. Thus, they are not necessarily water-repellent. They can be porous and as long as the exerted hydrostatic head is not high enough, they do not let the water passes through their pores such as camping tents or waterproof fabrics. In these examples, surface tension or free energy of the liquid is not directly involved, but the size of pores is important for sure. The smaller the pores, the harder the water can go through the surface of the fabric.^[145]

AR coatings definitely are not the only man-made products which have been improved by modifying their wettability. To take the advantage of hydrophobicity for many applications (such as in food packaging,^[150] antifouling membranes,^[151] automotive, aviation, marine, textile industries, cultural heritage conservation and restoration,^[152,153] etc.), especially having self-cleaning super-/ultrahydrophobic surfaces (Figure 8h), human beings like to take it to extremes, maximizing the CA. To do so, some limitations exist (to be termed “ultra-” and “superhydrophobic,” a surface must meet several requirements as will be discussed later),^[154] although myriad examples can be found in nature which possess extremely high CA.^[155] As a frame of reference, the static contact angles for some natural surfaces are provided in Table 4.

4.1.2. Superhydrophilic Self-Cleaning AR Coatings

Typical superhydrophilic surfaces have a water CA less than 10° (θ in Figure 8e shows a contact angle on a surface)^[156] [note: in different references, different contact angles are defined as superhydrophilic (less than 5° within 0.5 s or less)^[157]]. Basically, two types of superhydrophilic examples can be found among plant surfaces. The first group consists of plants which are permanently wet. Submerged water growing plants are in this group. Their surfaces are nearly smooth, almost without any sort of protuberances.^[158] This surface can repel oil droplet

in water, which indicates its potential for self-cleaning purposes.^[156] For example, the lotus plant has also been shown to exhibit superoleophobicity for its submerged parts.^[33] The second group is composed of plant surfaces which are able to absorb water due to their porous structure and multicellular hairs. This porous structure is able to absorb steam, condensation, dew, rain which can lead to antifogging property. The liquid–solid interface is usually governed by Wenzel model^[158] (Figure 8g). Some hydrophilic coatings, if exposed to sunlight, may also use chemical processes to break down undesirable organic materials to avoid fouling.^[152] Many products have been commercialized which can clean themselves based on photocatalysis together with water interaction with their hydrophilic surfaces. The pioneering material for this type of coating is TiO_2 , which can utilize UV light to decontaminate water.^[159]

To fabricate superhydrophilic AR coating aside from the obvious factor which is the material selection, porosity plays an essential role. If the porosity of the coating is almost equal or larger than the volume of the liquid which the coating is exposed to, the contact angle can reach zero.^[160] Table 5 shows an overview of some selected recent studies on superhydrophilic AR coatings.

When superhydrophilicity is added to AR coatings, at least two other favorable functions might be added with little extra effort – photocatalytic activity and antifogging. Also, it is interesting to note there are few other properties, such as antibacterial properties, that can arise when producing these materials.

Photocatalytic Activity: As mentioned earlier, TiO_2 coatings are the pioneer material for multifunctional AR coatings which can self-clean through a photocatalytic reaction. The superhydrophilicity in TiO_2 is induced by light.^[159] The details of the photocatalytic process can be found elsewhere,^[161] but, in general, any AR coating which has the outer layer made of this material can potentially put UV light to use.

Wang et al. fabricated an AR coating using tetraethyl orthosilicate (TEOS) and tetrabutyl orthotitanate (TBOT), and the $\text{SiO}_2/\text{TiO}_2$ bilayer coatings. They tested the photocatalytic activity of the coating by degrading methyl orange in an aqueous solution. The coating was exposed to UV light for 2 h which led to a superhydrophilic surface which could also degrade a 5 mg mL^{-1} solution of methyl orange by 43.6%.^[162] As another example, Du and He fabricated an AR coating on a soda lime glass substrate through hydrothermal NaOH etching. After introducing TiO_2 through dip-coating, they found that it was possible to effectively degrade methyl blue (10 mg L^{-1}) under UV light.^[163]

Antifogging: Fogging can be a big problem for ophthalmic lenses, windows, vehicles windshields, and architectural glazings. In high humidity or high-temperature environments, a glass interface which has temperature difference can attract condensation.^[107] As droplets grow and accumulate their diameters can quickly become larger than half of the shortest visible light wavelength (380 nm), $>190 \text{ nm}$, causing scattering. In extreme cases, this can result in a massive loss of transmission. However, as a surface phenomenon, fogging can be controlled by changing the material's affinity to water. This property can be introduced to a surface through either superhydrophilicity (uniform wetting) or superhydrophobicity (will be discussed later).^[164] Almost all of the papers which can be found through a simple Scopus search with “antifogging” and “antireflective” are

Table 5. Selected superhydrophilic AR coating studies.

Type/shape	Substrate	Fabrication	Contact Angle (CA) [°]	Transmission (T) [%]	Application	Reference
Nanopillar	Quartz	Reactive ion etching	≈0	>90% (550–1000 nm)	Optical devices, can add antibacterial	[258]
Three-layer (top layer dendrimer-like mesoporous silica nanoparticles)	Glass	Dip coating	Minimum near 2	Maximum 97.7% at 494 nm	Optical devices	[157]
Three-layer composite film (SiO ₂ and TiO ₂)	BK-7 glass	Dip coating	2	Average 99.4% (500–700 nm)	Solar cell panels, greenhouses, or architectural glasses	[259]
Macro-mesoporous SiO ₂ /TiO ₂	Glass	Growth + dip coating	<5 After UV irradiation	>90% (400–1200 nm)	Display devices, and PV cells	[260]
Nipple-like silica nanoparticles	Glass	Chemical vapor deposition	Minimum near 2	>90% (400–600 nm)	Self-cleaning AR coating	[261]
SWS	Fused silica	Reactive ion etching	≈0	>94% (500–1300 nm)- Double sided: maximum of 99.5% at 550 nm	Superhydrophilic AR coating	[262]
Mesostructured SiO ₂ + TiO ₂	Glass	Dip coating	Initially <5	Maximum of 96.9% at 620 nm	Solar cells, windowpanes, and eyeglasses	[263]
Porous	Glass	Vapor etching	3.2	Maximum of 99%	Large area AR coating	[264]
Raspberry-like SiO ₂ -TiO ₂	Glass	Layer-by-layer assembly	After calcination: superhydrophilic	Maximum of 97%	Self-cleaning surfaces with photocatalytic activity	[265]

instances of superhydrophilic AR coatings except for a report by Gao et al. on mosquitos *Culex pipiens* which have a nearly ideal superhydrophobic antifogging property in their compound eyes (Figure 9a,b).^[164]

Several patents related to antifogging coatings rely on surfactants. For example, Scholz and Tiers patented an antireflective and antifogging coating in 1996 which can enhance the light transmission by at least 3% over the uncoated substrate (tested at 550 nm). Their approach uses an inorganic metal oxide (preferably silica ideally 4–8 nm) together with particular hydrophilic anionic silane to create a relatively durable antifogging surface.

4.2. Superhydrophobic AR Coating

Earlier lotus leaf, *N. nucifera* was mentioned as the well-known embodiment of superhydrophobic surfaces in nature. As can be seen in Figure 8a–d, the leaf consists of “nubs” sticking out from the surface. The distance between the nubs is 20–40 μm and each nub is composed of smaller crystalloids made of hydrophobic wax with a rough surface.^[144] The irregularities at the microscale on lotus leaf surfaces are mainly the result of (hydrophobic) wax crystalloids. While the hydrophobicity of the lotus leaf has been known for centuries, the exact mechanism and structure were revealed with electron microscopy.^[165] Perhaps the first paper on a man-made self-cleaning surface dates back 1995.^[166] Since then, myriad research papers have been published and many commercial coatings/products have been produced such as Pilkington Activ (a dual-action self-cleaning glass),^[167] Lotusan (paints and coatings for facades),^[168] Neat (a self-cleaning glass),^[169] SUNCLEAN(R) (a self-cleaning glass),^[170] which have co-opted this idea from nature.

Superhydrophobic self-cleaning surfaces are more intriguing since water beads up and either slides or rolls-off, removing dirt and contaminants from the surfaces (Figure 9g). The lotus leaf is far from a singular material in this respect, Neinhuis and Barthlott reported a long list of plant species (more than 200) which exhibited liquid repellency.^[33]

A surface can be considered as superhydrophobic if its CA, θ , exceeds 150° (see Figure 8e,h). However, a static CA alone provides no guarantee of “self-cleaning.” Rose petals, as was discussed by Feng et al.,^[171] provide a counterexample wherein high adhesion forces prevent water droplets from moving. Thus, while droplets do not wet the surface (taking a near-perfect spherical shape), droplets do not roll-off rose petals, even when they are held upside down. This is called the “petal effect,” and it is much less useful for modern applications than the “lotus effect.”^[171] Thus, hysteresis and adhesion are two other significant factors to gauge for self-cleaning functionality. For many surfaces, it is best to measure the difference between the advancing and receding contact angle (see Figure 8i).^[172] If these are similar, then there is little adhesion and the surface is likely to self-clean. Moreover, the tilting angle, or the angle at which a water drop starts to move on a tilted surface, should be less than 10°^[158] for self-cleaning to work effectively. Even with these added boundaries, there are several natural materials which tend to exhibit both self-cleaning and antireflectivity. For some species of cicada, their wings are transparent, antireflective (≈2% reflectance in the visible region), and superhydrophobic.^[74,173] Although rare, the wings of some butterflies and moths (lepidopteran) are also nearly transparent except for small structural portions of their wings (their margins and veins) while also repelling water.^[174] To put this in context, the maximum transmission of these wings is nearly 98% across the wavelength range of 200–800 nm.^[16]

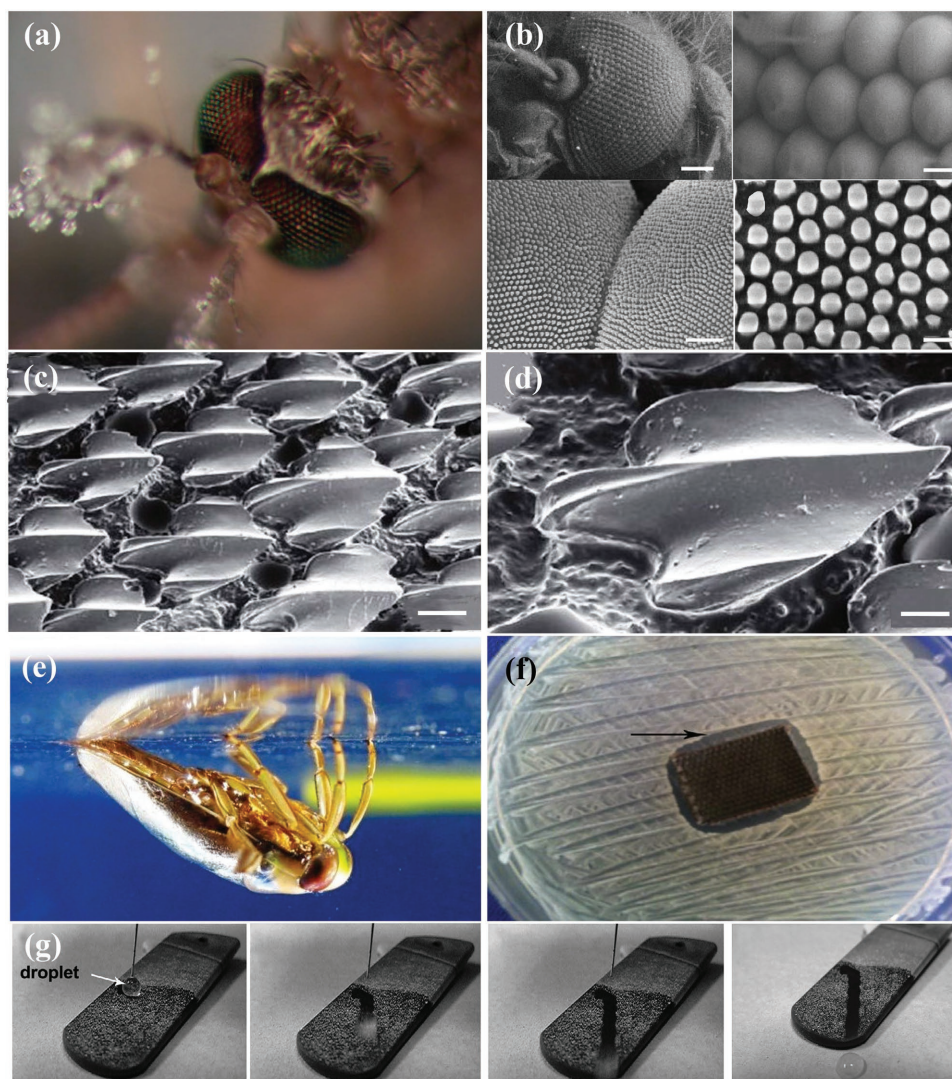


Figure 9. a) Antifogging mosquito eyes (in the presence of moisture, the eye surface is clear while the hairs nucleate some drops). b) SEM image of the mosquito eye (at different magnifications). Reproduced with permission.^[164] Copyright 2007, Wiley. c,d) SEM image of shark-skin replica patterned in Epoxy (45° tilt-angle top view – at different magnifications). Reproduced with permission.^[230] Copyright 2013, Wiley. e) Lateral view on the water bug *N. glauca*. Reproduced with permission.^[183] Copyright 2011, Beilstein-Institut. f) Antibacterial activity of modified cotton textiles (zone of inhibition is indicated by the arrow). Reproduced with permission.^[198] Copyright 2010, Elsevier. g) The self-cleaning behavior of a superhydrophobic surface. Reproduced with permission.^[231] Copyright 2013, Elsevier.

4.2.1. Fabrication of Superhydrophobic AR Coatings

Nature has taught us that superhydrophobicity is made possible by controlling surface energy via surface chemistry and/or micro-/nanostructures.^[175] Physical roughness itself can increase the surface area of the solid which decreases surface energy (e.g., Wenzel model – Figure 8g).^[147,176,177] Air trapped between water and the surface can form a kind of cushion to hinder surface wetting (e.g., the Cassie model – Figure 8f).^[176,178] If the water flows over these types of surfaces, it can skip or “slip” as it moves – e.g., with slip lengths of several micrometers possible in Cassie-state superhydrophobic surfaces.^[125] Superhydrophobic surfaces can be produced by either making a rough surface from low surface energy material

(i.e., a subtractive method) or by coating a rough surface with low surface energy materials (i.e., an additive method). Based on these two, numerous methods and materials for creating hydrophobic surfaces have been reported in recent years.^[33,125,144,146,179] For instance, fluorocarbons (e.g., Teflon), silicones (e.g. polydimethylsiloxane (PDMS)), and some inorganic materials (e.g., ZnO and TiO₂) have been of particular interest because of their extremely low surface energies.^[144]

Multifunctional superhydrophobic self-cleaning AR coatings have recently become feasible to produce in the laboratory as well. Since their fabrication techniques are so similar, and because topography and/or surface energy are of the main concern, it is possible to achieve geometries which are common in both. Both the moth’s-eye structure and porous AR coatings are

Table 6. Commercial coatings to change the contact angle via surface chemistry.

Compounds or product names	Quoted CA	Reference
Chlorosilanes such as:		[180]
octyl-trichloro-silane (OTS),	114° ± 2°	[266]
perfluorinated octyl trichloro silane (pFOTS)	122° & 156° (from gas phase)	[267]
Alkyltrichlorosilanes such as:		[180]
dodecyl trichloro silane (DTS),	(Advancing CA) 162°–176°	[268]
methyltrichlorosilane (MTS)	≤ 161°	[269]
Alkoxysilanes such as:		[180]
tetraethoxysilane (TEOS),	(for water) > 160°	[270]
perfluoro decyl triethoxy silane (PTES),	> 165°	[271]
n-octadecyl trimethoxy silane (ODS),	> 105°	[272]
trimethoxy silane,	155° ± 2°	[273]
tetramethoxy silane,	–	[180]
3-aminopropyl trimethoxy silane (APTMS)	(smooth surface) 77° < CA < 160° (rough surface)	[274]
Ceramic Pro Rain – Superhydrophobic coating for glass surfaces	110°–115°	[275]
Aquapel applicator pack	–	[276]
Rust-Oleum NeverWet liquid repelling treatment	165°	[277]
Hydrobead – super water-repellent spray	–	[278]

likely to have similar surface topography as is necessary for self-cleaning, but the surface chemistry is not necessarily aligned.

As regards the fabrication of these coatings, it may be possible to apply an optically thin superhydrophobic layer outside of the AR coating for protection. This is possible with a fluorocarbon-based coating applied to the AR coating via plasma deposition using CF₄ or CF or monolayer self-assembly from a liquid or gas phase.^[180] Table 6 presents some of the commercial coatings that may be used for this purpose.

Unfortunately, these superhydrophobic protective coatings can theoretically change the effective optical constants, leading to some changes in the reflection and transmission. Principally, there is a trade-off between antireflectivity and surface wetting which implies that suitable roughness is needed to achieve both the properties.^[181]

For example, Dou et al. studied a SiO₂ film using the sol-gel method. They treated their AR coating using 1H,1H,2H,2H-perfluorodecyltrichoxysilane (PFDS) to substitute the –OH groups on the surface to increase the contact angle by decreasing the surface energy. The coating reached the maximum transmittance of 97% with the treatment, significantly above the 95.7% observed in the absence of PFDS layer while the CA reached 130.6°.^[182] However, care must be taken to ensure hydrophobicity is not applied at the expense of higher reflection or lower transmission. This means achieving a high contact angle is conditional upon introducing roughness to these available materials.^[148] Table 7 shows an overview of some recent selected studies on superhydrophobic AR coatings.

4.2.2. Adding Even More Functionality

Controlling the contact angle can also bring some side benefits. Through the clever choice of the materials, the fabrication process, and other aspects of the design, it is possible to imbue at least one more level of functionality into these materials, if it is beneficial to the application. These characteristics can include drag reduction, oleophobicity, antimicrobiality, freeze resistivity, anticorrosivity, induced wettability changes, and many others.^[152] Although not many researchers have explicitly sought superhydrophobic AR coatings which possess such additional properties, they can certainly be found in nature (and independently in other man-made materials).

Drag Reduction: Ditsche-Kuru et al. studied a backswimmer bug, *Notonecta glauca* (Figure 9e). They observed a persistent air film on the upper side of the bug, irrespective of the hydrostatic and hydrodynamic conditions they commonly encounter (including submersion to significant depths). They also measured a friction reduction when the bug slides across the water created by this air film, indicating the bug effectively has a slip boundary with the water. The air in artificial hydrophobic surfaces usually lasts a few days, while the air film in a few plants and insects, which are considered semiaquatic, can last considerably longer. They highlighted the potential impact of applying this biomimetic lesson to reduce friction on ship hulls.^[183] Drag reduction is possibly the most useful attribute of superhydrophobic surfaces – outside of self-cleaning – seen in nature. As one example, some sharks have a mucus layer on their skin which creates localized hydrophobic areas that change the flow field around their riblet structures – structures which are aligned in the flow direction. These riblet structures on the outer skin of sharks (when swimming very fast) have been shown to decrease drag in the turbulent flow by ≈10%^[184] (Figure 9c,d). Researchers have been able to reproduce analogous structures with similar drag reductions for minimizing pumping energy in fluid flow applications.^[184] Fish scales, rice leaves, and butterfly wings have also been reported to have drag reduction and self-cleaning properties.^[185] Along these lines, there are some commercialized products which make use of superhydrophobic surfaces for drag reduction, such as Speedo Fastskin racing swimsuits^[186] (noting that full body suits have now been banned from the 2012 and 2016 Olympics for simply being too good^[187]). Thinking even more broadly, any application in which transparent AR coatings are to be exposed to a moving fluid (e.g., reduced fuel use in transportation, dynamic wind load reduction from on building windows, performance swimming goggles, etc.), drag reduction might prove beneficial.

Induced Wettability Changes: An interesting property which can be found in some materials is the ability to change wettability through an external stimulus such as light irradiation, electrical potential, temperature, pH, or selected solvents, and mechanical forces – reversibly. Although responsive wettability can also be found on flat surfaces, to improve this property, these surfaces are usually composed of a combination of a hydrophobic or hydrophilic material with a textured surface.^[188] A photoresponsive wettability can be found among some inorganic materials such as TiO₂, Ga₂O₃, WO₃, ZnO, V₂O₅, SnO₂, etc. This property has been also reported for some organic materials. There are some instances of UV-induced switchable

Table 7. Overview of selected recent transparent superhydrophobic and/or AR coatings reported in the literature.

Base material(s)/ type or shape	Substrate	Modification agent	Fabrication	CA [°]	Transmission (T) [%]	Reference
Silica nanoparticles (SNPs)/porous	Glass slides and fused silica	Hexamethylsilazane (HMDS)	Dip coating	Fused silica: max. 147 Glass slide: max. 155	Max. T ≥ 98.79	[279]
ZnO, indium tin oxide (ITO), and silane-modified SiO ₂ , nanoparticles/porous	Soda lime glass, polycarbonate, and poly(methyl methacrylate) (PMMA)	Octadecylphosphonic acid (ODP) for ZnO and ITO.	Dip coating	ZnO on polycarbonate was the highest: 169	ITO on PMMA was the highest: 97	[280]
Al-doped ZnO/nanorods	Glass	1H,1H,2H,2H-perfluorodecyltriethoxysilane (PFDTES)	Radio frequency (RF) sputtering and self-assembly	Advancing CA for doped with Al ≈ 155	Only the reflectance at normal incidence was studied	[281]
Silica nanoparticles/porous	Glass slide	1H,1H,2H,2H-perfluorooctyltriethoxy silane (POTS)	Dip coating and CVD ^{a)}	157.8	Max. T: 96.2	[215]
Silica particles/cicada-wing-inspired	Poly(ethylene terephthalate) (PET)	(tridecafluoro-1,1,2,2-tetrahydrooctyl)-trichlorosilane	RIE ^{b)} , wet etching, and CVD	Max. 156.9	>95 (600–900 nm) (2 min RIE)	[282]
Hollow silica nanoparticles/porous	Glass	1H,1H,2H,2H-perfluorooctyl-trichlorosilane (CF ₃ (CF ₂) ₅ CH ₂ CH ₂ SiCl ₃) (PFTS)	Dip coating and CVD	162	Average: 95 (530–1340 nm) Visible reached 97 (400–800 nm)	[219]
CaF ₂ /nanograss (NG)	Glass	polytetrafluoroethylene (PTFE)	GLAD ^{c)} and dip coating	Advancing CA > 150	Only reflectance was studied	[88]

^{a)}CVD: chemical vapor deposition; ^{b)}RIE: reactive ion etching; ^{c)}GLAD: glancing angle vapor deposition.

wetting AR coatings. For example, Suresh Kumar et al.^[189] fabricated ZnO nanostructured on poly(ethylene terephthalate) (PET) (around 30 nm spherical nanoparticle-shaped), ITO, and glass. On ITO and glass, the resulting spindle- and flower-like structures were in the 100–500 nm range – e.g., the spindles had a central diameter of nearly 200–300 nm, but the width and length were 150 and 500 nm, respectively. Using these designs, apart from their antireflectivity, enabled photoinduced switching between hydrophilic and hydrophobic states. They proved this attribute by measuring contact angle. Generally, in ZnO films, wettability can change from hydrophobicity to hydrophilicity by the exposure of UV light which forms electron–hole pairs on the surface of ZnO. Lattice oxygen can react with some of the generated holes, resulting in surface oxygen vacancies. Simultaneously, through a dissociative mechanism, oxygen and water might compete to adsorb on vacancies. Kinetically, –OH groups are more likely to be adsorbed on the defective sites compared to oxygen. If the ZnO film is protected in dark place, gradually oxygen atoms can take –OH group positions.^[189]

Electrowetting is another common means to switch wettability of a surface. By applying a voltage between the substrate and a droplet, it is possible to transition between states.^[190] Thermal responsive wetting can also be reversible in some polymeric materials.^[191] This has proven valuable in separation processes such as air filtration, oil–water separation, etc. pH or solvent responsive wetting been used in drug delivery, sensing, enzyme immobilization.^[190] Finally, stress-responsive wetting can be induced by exerting a mechanical force to change a flexible/elastic structure, such as curvature forming.^[192] Overall, having the ability to switch between states might prove valuable to transparent surfaces that frequently interact with water and humidity.

Oleophobicity: Although they seem somewhat incompatible, there are some examples of superhydrophobic surfaces

which are also superoleophobic. Fish scales contain mucus, protein, and calcium phosphate to make them resistant to oil contaminations in water.^[33] Organic liquids have commonly lower surface tensions than water. For example, hexadecane shows a very low apparent CA on a lotus leaf which is one of the best superhydrophobic surfaces in nature. Therefore, apart from surface roughness and chemistry, there should be another factor to consider. Tuteja et al. designed some superhydrophobic and superoleophobic surfaces with re-entrant curvature (concave) in which they argued that there are two parameters which can affect oleophobicity of these geometries, spacing ratio and robustness parameters which reflect the stability of metastable Cassie state according to the liquid properties.^[193] In another study, Wang et al. fabricated superhydrophobic and superoleophobic fabrics made of fluorinated-decyl polyhedral oligomeric silsesquioxane and a fluorinated alkyl silane. They reported high CAs for water (171°), hexadecane (155°), and tetradecane (152°).^[194]

Dutriez et al. reported a transparent polymeric AR coating based on poly(methyl methacrylate-*r*-glycidylmethacrylate)-*b*-poly(perfluorooctylethyl methacrylate) (PMGMA-PFMA) on glass which had water and oil-repellent properties due to the presence of fluorine-containing PFMA.^[195] In another study, Zhang et al. fabricated organically modified silicate AR coating on BK-7 glass which was shown to possess water and oil resistivity through checking the CA of water, CH₂I₂, and polydimethyl siloxane on the coating because of presence fluorine content.^[196] Kontziampasis et al. fabricated a superhydrophobic AR coating on glass made of PMMA through plasma processing which showed oleophobicity. They tested this property by measuring the CA of oily water which contained surfactant.^[180] Joki-Korpela et al. reported UV curable polyacrylate antireflective structure replicated on PMMA which also proved to have water and oil-repellent properties by measuring water and oleic acid CA on the coating.^[197]

Antimicrobial/Fouling: It has been found that cells and bacteria are less able to adhere to surfaces with very low surface energy. Thus, superhydrophobic surfaces can also be used to avoid biogrowth and biofouling – an extremely useful aspect for biomedical devices.^[153] Khalil-Abad and Yazdanshenas designed superhydrophobic antibacterial cotton textiles made by using silver particles. They tested the biological activity of their samples by inhibiting the growth of *Escherichia coli* (ATCC 25923, Gram-negative bacterium) and *Staphylococcus aureus* (ATCC 25922, Gram-positive bacterium) (Figure 9f).^[198] These reports are in line with studies on membrane separation studies which show superhydrophobic surfaces avoid fouling.^[151] Pogodin et al. (wings of clanger cicada, *Psaltoda claripennis*)^[199] and Ivanova et al. (wings of the dragonfly *Diplacodes bipunctata*)^[200] in two different reports showed the bactericidal property of cicada wings which were discussed earlier for their interesting optical and wettability features. On the man-made transparent superhydrophobic AR surfaces, rarely can papers be found in which bactericidal property has been studied.

Icephobicity: Although superhydrophobic surfaces are not always ice-repellant,^[201] this quality in some superhydrophobic surfaces can make them useful for some technologies which are deployed in cold or variable climates.^[202] For airplanes at high altitudes, mountain wind turbine blades, overhead power cables, and solar panels, ice can be a serious threat, leading to catastrophic failures.

Jung et al. found that surface roughness played a role in the freezing delay. They observed that surfaces, regardless of their wettability, can repel ice if they have smaller roughness. Moreover, larger contact angle means that less liquid is likely to stay on a surface to form ice. Therefore, material selection is the key to creating a surface which serves the dual function of being superhydrophobic and “icephobic” at the same time.^[203]

Boinovich and Emelyanenko analyzed the physiochemical mechanisms which affect anti-icing performance of superhydrophobic surfaces. They pointed out reducing heat transfer (e.g., contact area) between a water droplet and the surface can delay water droplet crystallization. To remove the droplet from the surface, self-cleaning must be in full effect, with near zero hysteresis in the advancing/receding contact angle and a high enough surface slope angle for the droplet to roll-off. Alternatively, if ice freezes on the surface, low adhesion could still enable ice crystals to be removed by wind, gravity, or other forces.^[204]

Wang et al. prepared four aluminum surfaces with different wettabilities through etching and coating with perfluorodecyltriethoxysilane (PTES). They used a temperature environmental chamber to control relative humidity at $-10\text{ }^{\circ}\text{C}$ while conducting ice adhesion tensile strength tests. An etched superhydrophobic sample coated with PTES showed icephobicity throughout the experiment except for the situation where relative humidity was 90%. In this condition, some local oversaturated regions were detected.^[205] While there has not been a lot of work on superhydrophobic AR coatings which possess ice repellency as yet, there are many transparent materials which would like to avoid the buildup of ice.

Anticorrosivity: Another interesting additional functionality that may be added to these materials is anticorrosivity. This property has, out of necessity, been incorporated into historical

artifacts for preservation. Manoudis et al.^[206] report an inexpensive way to spray coat monuments with superhydrophobic surfaces to preserve them. They used siloxane dispersions of nanoparticles such as SiO_2 , SnO_2 , TiO_2 , and Al_2O_3 which effectively changed the wettability of three different types of stone in a castle in Prague.^[206] Similarly, Stranges et al. proposed two different methods to protect ceramic artifacts through coating a transparent layer of TiO_2 . This layer made the artifacts hydrophobic and helped to inhibit corrosion from exposure to moisture and salt water.^[207] Chen et al. reported an antiscratch zeolite AR coating on glass which could show a quite high CA after modifying with hexamethyl disilazane (HMDS). They claimed solar application for their coating.^[134] However, strictly speaking, their coating cannot be considered as superhydrophobic because the reported water CA was just larger than 130° .

5. Testing of Surface Coatings

Considering the final application means that the material's performance in real (or accelerated) environmental conditions should be established. In particular, a major barrier for extensive practical application of nanocoatings is durability. As can be seen in Figure 2, AR coatings are useful in many distinct applications. Each application can impose different criteria and extra limitations on AR coatings. This fact has forced man-made AR coatings to take on a wide range of materials and designs. Although often neglected during the conception of a new material synthesis method, similarly, the durability of the AR coatings is critical. Ideally, AR coatings should last long enough to meet the demands of their application. However, some intrinsic factors (related to the physical and chemical properties of materials and process of the fabrication) and extrinsic factors (related to ambient conditions and the interaction of AR coatings with them) can shorten their working life. For example, AR coatings need to be tough enough to survive periodical soiling, cleaning, and diurnal temperature swings. Environmental factors such as moisture can lead to fogging, which can also affect performance, even if the AR itself is unaffected.^[164]

5.1. Durability Tests of Surface Coatings

To determine if AR coatings are reliable, several tests have been devised. Jorgensen et al. tested several AR glazings inside environmental chambers which use harsh conditions (elevated temperature and humidity) to simulate in-service conditions. Surprisingly, when compared with the real-world operation, Jorgensen et al. found that AR glazings in the chambers experienced less degradation. They concluded that the accumulation of dust and dirt during outdoor tests was more important than temperature and humidity.^[208]

Thin film adhesion tests can be conducted to determine the bond strength/uniformity. These can be categorized as a scratch, pull, and peel tests, among others. In a scratch test, a smooth but finely pointed object is employed to strip the coating from the substrate or leave a clear channel on the film.^[209] Detailed information on the scratch test and mechanical properties' measurement of a thin film can be found in

a review by Malzbender et al.^[210] For pull tests, there are two ways to measure thin film adhesion. First, the “topple test” involves sticking a rod or cylinder to the film and separating it by exerting lateral force to detach the film from the substrate. Alternatively, the “direct pull” method can be used to measure the tensile force to pull the film from the substrate through applying a force perpendicular to a cylinder which has bonded to the film.^[209,211,212]

Vacuum-deposited films usually experience a temperature increase at their surfaces which leads to considerable internal stresses, and perhaps delamination. The peel test gives a qualitative and quantitative way to measure these stresses through the peeling force.^[211]

Another test which can be done is a buckling (bending) test to measure the elastic modulus of thin films. When a thin film is bent, cracks form due to exceeding the critical tensile stress of the film. Wu et al. used a buckling test to determine the durability of a sol-gel coating on a polycarbonate substrate.^[213] Stafford et al. introduced a rapid and reliable technique to measure the elastic modulus of soft coatings.^[214]

In addition to adhesion tests, several other tests have been developed to measure different aspects of durability and reliability for the application. A key focus of these efforts is on “accelerated” testing, where materials are exposed to harsh conditions, in excess of their real applications. As an example, accelerated tests have been proposed to simulate the effect of rain by using a water jet.^[215] As another example, researchers have conducted sand abrasion tests,^[215–217] wherein a coated film is exposed to the high-speed collision of sand grains from different heights (e.g., increasing kinetic energy). The maximum height from which sand can be dropped without harming the film represents the erosion durability.^[216]

Alternatively, some researchers have elected to simply go for long-term studies in which performance of AR coatings was studied under normal conditions in their application environment.^[208,215,218] The American Society for Testing and Materials (ASTM) has specified durability tests specifically for AR coatings, with **Table 8** summarizing the standard procedures.

Thermal stability represents another critical aspect of durability, although this is infrequently tested since many applications do not experience high temperatures. In a study by Xu et al., however, a multifunctional AR coating was tested up to 350 °C. The coating and the substrate were annealed for 2 h at different temperatures from 100 to 350 °C. Xu et al. found that their AR coating could maintain its properties up to 300 °C.^[219]

Along with these tests based on the literature, some tests related to wettability/nonwettability should be conducted to compare the coatings before and after each test mentioned above as instances. For example, in literature, static contact angle, roll-off behavior, contact angle hysteresis, and other measures were reported as the certification criteria.^[220]

Obviously, there is no “one-size-fits-all” approach, and some of these tests will be more useful for a given application than others. As an example, a material may be very durable at high temperature, but breaks down easily under the UV light of concentrated solar applications. The durability of this coating should be tested and certified so that it can survive the harsh conditions of its application. Therefore, standard tests should be selected based on the application.

Table 8. ASTM durability tests for AR coatings.

Test title	Purpose	Procedure	Reference
ASTM D4828-92	Mechanical washing test	Wash the coating for up to 100 cycles using a sponge (50 cycles min ⁻¹).	[210]
ASTM D870-09	Hot water immersion test	Immerse the coating in deionized (DI) water and heat to 85 °C for 100 h.	[283]
ASTM B117	Salt spray test	Expose the coating to fog produced by atomization of 5% NaCl solution for 100 h.	[283]
ASTM D6943	Acid immersion test	Immerse coated samples in a 100 × 10 ⁻³ M H ₂ SO ₄ solution at 35 °C for 100 h.	[283]
ASTM D3359-02	Scratch test	Move pencils with various grades (1H–6H) over the coated samples at a 45° angle to the horizontal with a force of 7.5 ± 0.1 N. The grade of the pencil which damages/scratches the AR coating sample on glass substrate defines the scratch hardness (e.g., “2H” hardness).	[283]

6. Fabrication Costs

Cost is clearly a major concern for the industry, particularly for large-area applications. The price of producing single and multifunctional coatings depends on the raw material price, the fabrication process, labor, surface modification method, and other balance of system/integration costs. The range of “acceptable” prices can vary a lot between applications. For example, biomedical devices have a much higher price point (on a \$ m⁻² basis) than architectural glazing or photovoltaics.^[54] In fact, photovoltaics module prices have fallen below 1000 USD m⁻² today,^[221] so there is not much margin to add costly AR or multifunctional coatings (although some have been produced – e.g., a porous AR coating with refractive index of nearly 1.22 on the panel^[60]). Studies have shown that AR coatings can provide positive net present value in greenhouses or photovoltaics if their added cost can be less than \$7.5 m⁻² or less than \$14 m⁻², respectively.^[208] This is well below the cost of many of the commercially available AR products on the market. As one example, a top-of-the-line broadband AR coating (with <0.5% reflection of visible light) on float glass (304.8 × 254 mm) costs ≈1000 USD m⁻² from Edmund Optics.^[222] For large-scale applications, the OptiView AR glass from Viracon costs \$15 ft⁻² (or, ≈160 USD m⁻²).^[223] Based on this, it seems if AR coating costs need to be reduced by nearly an order of magnitude before they could be integrated into large area, modern transparent materials. Among the myriad AR coating fabrication techniques,^[53,74,224] it seems that sol-gel (dip coating) and nanoimprint lithography (NIL) represent the most cost-effective pathways for moving toward implementing large-scale AR coatings.^[54,60,225] Hobbs et al.^[55] stated that AR coatings should be beneficial for applications where the main use occurs at less than 30° incident angle range from the normal, over less than 1 octave of bandwidth (e.g., 400–700 nm, 800–1100 nm, 1.5–1.6 μm, 3–5 μm, 8–12 μm), in a nonabrasive environment (no erosion), and

at low temperature and humidity. Additionally, AR coatings are more suited to low optical fluence applications (e.g., $<20 \text{ J cm}^{-2}$ for fused silica optics), and those with low radiation levels (e.g., $<300 \text{ kRad Si}$ proton exposure).^[55] Even with all of these constraints in place, reliable, low-cost AR coatings would still be beneficial for most of the applications shown in Figure 2.

7. Conclusions and Future Directions

Man-made antireflective coatings which incorporate other functionalities have advanced rapidly in recent years due to our ability to mimic and improve upon designs found in nature. From this literature review, it is clear that achieving multifunctional (AR+) designs which are durable and produced using low-cost fabrication techniques would represent true biomimicry, but this may yet be several years into the future. Broadband, omnidirectional, AR coatings which can self-clean are needed, but the literature reveals only a few pioneering forays into how we might cost-effectively achieve these for windows, displays, and solar collectors. Although man-made materials have surpassed many nature materials as far as individual properties, such as reflectivity or preferential wettability, nature is still the clear leader in stacking multiple properties together in a way which is best-suited to real-world conditions.

On the fabrication side, the technological gap between how nature makes and maintains its materials and what we can do in the lab is still large. All natural AR+ self-cleaning surfaces (in plants or animals) are made below 40°C . In the laboratory, however, much higher temperatures (e.g., $200\text{--}400^\circ\text{C}$) are often required. Biology uses “green” chemistry with nontoxic materials, whereas many of the reactants and products involved in AR and self-cleaning fabrications are often acutely toxic. Aside from the environmental impacts associated with these limitations, these issues are a big source of manufacturing cost. Thus, nature still has some lessons for us regarding low-impact and low-cost fabrication.

Dip coating, spray pyrolysis, and 3D printing might be the most cost-effective near-term options for synthesis going forward, but these still suffer from technical limitations. Film uniformity can be a common problem in dip coating and spray pyrolysis. In 3D printing, the resolution and refractive indices of transparent materials represent the limiting factors. Some companies, such as Nanoscribe (<http://www.nanoscribe.de/en/>), are trying to overcome this by moving toward systems which can 3D-print features on the sub-micrometer scale, but it is yet to be seen if this will be cost-effective.

Based on the available literature to date, there is certainly room for improvement and further insights to be gained from nature on robustness, reliability, and durability for multifunctional transparent surfaces. For instance, since solar collectors have a life of 25+ years, they need to be able to maintain transmission and, withstand regular exposure to dust and contaminants, and repel water for their entire life span. For transparent surfaces, nature may yet teach to slash production costs or ways of self-repairing which could make advanced, multifunctional transparent surfaces commercially viable.

Acknowledgements

This research was funded by the Australian Research Council (ARC) (ARC – DE160100131). The authors would also like to thank the School of Mechanical and Manufacturing Engineering at the UNSW Sydney for supporting this work. Finally, M.M. would like to thank Mehdi Rafeie for his helpful discussion on figure preparation.

Conflict of Interest

The authors declare no conflict of interest.

Keywords

antireflective coatings, durability, multifunctional coatings, self-cleaning, transparent surfaces

Received: January 23, 2018

Revised: March 14, 2018

Published online:

- [1] I. Terashima, T. Fujita, T. Inoue, W. S. Chow, R. Oguchi, *Plant Cell Physiol.* **2009**, *50*, 684.
- [2] C. Akerlind, H. Arwin, T. Hallberg, J. Landin, J. Gustafsson, H. Kariis, K. Järrendahl, *Appl. Opt.* **2015**, *54*, 6037.
- [3] V. R. Binetti, J. D. Schiffman, O. D. Leaffer, J. E. Spanier, C. L. Schauer, *Integr. Biol.* **2009**, *1*, 324.
- [4] G. S. Watson, J. A. Blach, *SPIE Smart Materials II*, Vol. 4934, SPIE, Melbourne, Australia **2002**.
- [5] A. Blagodatski, A. Sergeev, M. Kryuchkov, Y. Lopatina, V. L. Katanaev, *Proc. Natl. Acad. Sci. USA* **2015**, *112*, 10750.
- [6] A. R. Parker, H. E. Townley, *Nat. Nanotechnol.* **2007**, *2*, 347.
- [7] A. Gombert, B. Bläsi, in *Functional Properties of Bio-Inspired Surfaces: Characterization and Technological Applications* (Eds: E. A. Favret, N. O. Fuentes), World Scientific, Singapore **2009**, Ch. 4.
- [8] Seashell Armor Could Offer Transparent Protection for Troops, <http://www.livescience.com/44484-seashell-armor-for-troops.html> (accessed: May 2017).
- [9] S. Johnsen, *Biol. Bull.* **2001**, *201*, 301.
- [10] G. Agez, C. Bayon, M. Mitov, *Acta Biomater.* **2017**, *48*, 357.
- [11] H. A. Macleod, *Thin-Film Optical Filters*, 4th ed., Taylor & Francis Group, CRC Press, FL, USA **2001**.
- [12] M. N. Polyanskiy, Refractive index database, <http://refractiveindex.info/> (accessed: December 2016).
- [13] S. A. Boden, D. M. Bagnall, *Prog. Photovoltaics* **2009**, *17*, 241.
- [14] J. D. Meador, D. J. Guerrero, G. Xu, X. Shao, N. Dobson, J. Claypool, K. Nowak, *Microlithography*, Vol. 3678, SPIE, CA, USA **1999**.
- [15] P. Spinelli, M. Verschuuren, A. Polman, *Nat. Commun.* **2012**, *3*, 692.
- [16] A. Yoshida, M. Motoyama, A. Kosaku, K. Miyamoto, *Zool. Sci.* **1997**, *14*, 737.
- [17] M. H. Abdullah, L. N. Ismail, M. R. Mahmood, in *Advanced Materials Research* (Eds: M. H. Mamat, Z. Khusaimi, S. A. Bakar, A. M. Nor, T. Soga, M. R. Mahmood), Vol. 832, Trans Tech Publications, Aedermannsdorf, Switzerland **2014**.
- [18] K. Abe, Y. Sanada, T. Morimoto, *J. Sol-Gel Sci. Technol.* **2001**, *22*, 151.
- [19] SCHOTT Glass Made of Ideas, <http://www.us.schott.com/english/index.html> (accessed: February 2017).
- [20] S.-G. Lee, J.-s. Choi, J.-E. Kim, H. Y. Park, C.-S. Kee, *Opt. Express* **2008**, *16*, 4270.

- [21] A. Kano, A. R. Rouse, A. F. Gmitro, *J. Biomed. Opt.* **2013**, *18*, 016013.
- [22] D. Brodoceanu, R. Elnathan, B. Prieto-Simón, B. Delalat, T. Guinan, E. Kroner, N. H. Voelcker, T. Kraus, *ACS Appl. Mater. Interfaces* **2015**, *7*, 1160.
- [23] P. Y. Baroni, B. Päivänranta, T. Scharf, W. Nakagawa, M. Roussey, M. Kuittinen, H. P. Herzig, *J. Eur. Opt. Soc.* **2010**, *5*, 10006.
- [24] X. Ye, X. D. Jiang, J. Huang, L. X. Sun, F. Geng, Z. Yi, X. T. Zu, W. D. Wu, W. Zheng, *Opt. Laser Eng.* **2016**, *78*, 48.
- [25] A. Hiraki, H. Hiraki, in *Wide Bandgap Semiconductors: Fundamental Properties and Modern Photonic and Electronic Devices* (Eds: T. Kiyoshi, Y. Akihiko, S. Adarsh), Springer-Verlag, Berlin, Germany **2007**, Ch. 4.3.
- [26] R. E. Smallman, R. J. Bishop, *Modern Physical Metallurgy and Materials Engineering*, 6th ed., Elsevier, Butterworth-Heinemann, Stoneham, MA, USA **1999**.
- [27] a) C. Terrier, J. Chatelon, J. Roger, *Thin Solid Films* **1997**, *295*, 95; b) D. J. Thouless, *Phys. Rep.* **1974**, *13*, 93; c) D. Weaire, M. Thorpe, *Phys. Rev. B* **1971**, *4*, 2508.
- [28] M. Grätzel, *Nature* **2001**, *414*, 338.
- [29] R. G. Gordon, *MRS Bull.* **2000**, *25*, 52.
- [30] D. Ghosh, L. Martinez, S. Giurgola, P. Vergani, V. Pruneri, *Opt. Lett.* **2009**, *34*, 325.
- [31] D. S. Ghosh, *Ultrathin Metal Transparent Electrodes for the Optoelectronics Industry*, Springer Theses, Springer, Berlin **2013**.
- [32] W. Barthlott, C. Neinhuis, *Planta* **1997**, *202*, 1.
- [33] M. N. Valipour, F. C. Birjandi, J. Sargolzaei, *Colloids Surf., A* **2014**, *448*, 93.
- [34] Z. Guo, W. Liu, *Plant Sci.* **2007**, *172*, 1103.
- [35] T. Sun, L. Feng, X. Gao, L. Jiang, *Acc. Chem. Res.* **2005**, *38*, 644.
- [36] T. Khudiyev, T. Dogan, M. Bayindir, *Sci. Rep.* **2014**, *4*, 4718.
- [37] R. H. Siddique, G. Gomard, H. Hölscher, *Nat. Commun.* **2015**, *6*, 6909.
- [38] B. Rigby, *Nature* **1968**, *219*, 166.
- [39] D.-E. Nilsson, L. Gislén, M. M. Coates, C. Skogh, A. Garm, *Nature* **2005**, *435*, 201.
- [40] J. Strugnell, M. Norman, A. J. Drummond, A. Cooper, *Curr. Biol.* **2004**, *14*, R300.
- [41] W. E. Duellman, J. C. Señaris, *Herpetologica* **2003**, *59*, 247.
- [42] C. Schittich, G. Staib, D. Balkow, M. Schuler, W. Sobek, *Glass Construction Manual*, Walter de Gruyter, Germany **1999**.
- [43] a) L. L. Beecroft, C. K. Ober, *Chem. Mater.* **1997**, *9*, 1302; b) L. Martinu, D. Poitras, *J. Vac. Sci. Technol., A* **2000**, *18*, 2619; c) A. Cannavale, F. Fiorito, M. Manca, G. Tortorici, R. Cingolani, G. Gigli, *Build. Environ.* **2010**, *45*, 1233.
- [44] J. Deubener, G. Hensch, A. Moiseev, H. Bornhöft, *J. Eur. Ceram. Soc.* **2009**, *29*, 1203.
- [45] R. O. Claus, Y. Liu (Virginia Tech Intellectual Properties Inc, Nanosonic Inc), *US6316084B1*, **2001**.
- [46] H. Kang, S. Jung, S. Jeong, G. Kim, K. Lee, *Nat. Commun.* **2015**, *6*, 6503.
- [47] D. J. Lipomi, M. Vosgueritchian, B. C. Tee, S. L. Hellstrom, J. A. Lee, C. H. Fox, Z. Bao, *Nat. Nanotechnol.* **2011**, *6*, 788.
- [48] K. Chopra, S. Major, D. Pandya, *Thin Solid Films* **1983**, *102*, 1.
- [49] G. Thomas, *Nature* **1997**, *389*, 907.
- [50] A. Ç. Yunus, J. G. Afshin, *Heat and Mass Transfer*, McGrawHill, New York, USA **2007**.
- [51] M. Magnuson, C. F. Hague, *J. Electron. Spectrosc. Relat. Phenom.* **2004**, *137–140*, 519.
- [52] D. W. Ball, *The Basics of Spectroscopy*, Vol. 49, SPIE Press, WA, USA **2001**.
- [53] H. K. Raut, V. A. Ganesh, A. S. Nair, S. Ramakrishna, *Energy Environ. Sci.* **2011**, *4*, 3779.
- [54] P. Buskens, M. Burghoorn, M. C. D. Mourad, Z. Vroon, *Langmuir* **2016**, *32*, 6781.
- [55] D. S. Hobbs, B. D. MacLeod, J. R. Riccobono, *Defense and Security Symp.*, Vol. 6545, SPIE, FL, USA **2007**.
- [56] R. Jacobsson, J. O. Mårtensson, *Appl. Opt.* **1966**, *5*, 29.
- [57] B. T. Liu, W. D. Yeh, *Thin Solid Films* **2010**, *518*, 6015.
- [58] a) K. W. Meissner, *J. Opt. Soc. Am.* **1941**, *31*, 405; b) J. F. Mulligan, *Am. J. Phys.* **1998**, *66*, 797.
- [59] a) J. Falnes, *Mar. Struct.* **2007**, *20*, 185; b) S.-H. Yu, J.-S. Hu, *IEEE/ASME Trans. Mechatronics* **2001**, *6*, 483.
- [60] W. Glaubitt, P. Löbmann, *J. Eur. Ceram. Soc.* **2012**, *32*, 2995.
- [61] P. Löbmann, in *Chemical Solution Deposition of Functional Oxide Thin Films* (Eds: T. Schneller, R. Waser, M. Kosec, D. Payne), Springer, Wien, Austria **2013**.
- [62] J. Cox, G. Hass, A. Thelen, *J. Opt. Soc. Am.* **1962**, *52*, 965.
- [63] T. Schultz, M. Rankin, *J. Exp. Biol.* **1985**, *117*, 87.
- [64] S. Kinoshita, *Structural Colors in the Realm of Nature*, World Scientific, Singapore **2008**.
- [65] H. Sumita (Minolta Co Ltd), *US3781090 A*, **1973**.
- [66] S. Bruynooghe, M. Helgert, M. Challier, D. Tordova, M. Sundermann, T. Koch, A. Gatto, M. Schulze, E. B. Kley, *SPIE Nanoscience + Engineering*, Vol. 9558, SPIE, CA, USA **2015**.
- [67] A. Rehmer, K. Scheurell, E. Kemnitz, *J. Mater. Chem. C* **2015**, *3*, 1716.
- [68] Y. Song, J. Oh, *Sol. Energy Mater. Sol. Cells* **2016**, *144*, 159.
- [69] C. H. Chuang, D. M. Lu, P. H. Wang, W. Y. Lee, *DTIP*, IEEE, Budapest, Hungary **2016**.
- [70] A. Thelen, *Design of Optical Interference Coatings*, McGraw-Hill, New York, USA **1989**.
- [71] Y. Y. Liou, Y. T. Liu, *Jpn. J. Appl. Phys., Part 1* **2005**, *44*, 163.
- [72] A. Premoli, M. L. Rastello, *Appl. Opt.* **1994**, *33*, 2018.
- [73] A. Tikhonravov, M. Trubetskov, G. DeBell, *Appl. Opt.* **2007**, *46*, 704.
- [74] S. Chattopadhyay, Y. F. Huang, Y. J. Jen, A. Ganguly, K. H. Chen, L. C. Chen, *Mater. Sci. Eng., R* **2010**, *69*, 1.
- [75] S. Larouche, L. Martinu, *Appl. Opt.* **2008**, *47*, C219.
- [76] a) The ESSENTIAL MACLEOD, <https://www.thinfilcenter.com/> (accessed: February 2017); b) Virtual Lab Fusion, <http://www.lighttrans.com/> (accessed: February 2017); c) OptiLayer Thin Film Software, <http://www.optilayer.com/> (accessed: February 2017); d) Software Spectra, <http://www.spectra.com/> (accessed: February 2017); e) FreeSnell, <http://people.csail.mit.edu/jaffer/FreeSnell/freesnell.html> (accessed: February 2017).
- [77] E. D. Palik, *Handbook of Optical Constants of Solids*, Vol. 1, Academic Press, San Diego, CA, USA **1998**.
- [78] B. S. Chiou, J. H. Tsai, *J. Mater. Sci.: Mater. Electron.* **1999**, *10*, 491.
- [79] S. Ji, M. Ponting, R. S. Lepkowitz, A. Rosenberg, R. Flynn, G. Beadie, E. Baer, *Opt. Express* **2012**, *20*, 26746.
- [80] G. Beadie, J. S. Shirk, A. Rosenberg, P. A. Lane, E. Fleet, A. Kamdar, Y. Jin, M. Ponting, T. Kazmierczak, Y. Yang, *Opt. Express* **2008**, *16*, 11540.
- [81] L. Rayleigh, *Proc. London Math. Soc.* **1879**, *1*, 51.
- [82] W. H. Southwell, *Opt. Lett.* **1983**, *8*, 584.
- [83] A. J. Nolte, M. F. Rubner, R. E. Cohen, *Langmuir* **2004**, *20*, 3304.
- [84] H. Bartsch, S. Lange, P. Frach, K. Goedicke, *Surf. Coat. Technol.* **2004**, *180–181*, 616.
- [85] K. Senda, T. Matsuda, T. Kawanishi, K. Tanaka, H. Usui, *Jpn. J. Appl. Phys.* **2013**, *52*, 05DB01.
- [86] M. S. Wang, L. Yang, X. J. Huang, *IEEE Electron Device Lett.* **2014**, *35*, 464.
- [87] H. K. Raut, S. S. Dinachali, K. K. Ansah-Antwi, V. A. Ganesh, S. Ramakrishna, *Nanotechnology* **2013**, *24*, 505201.
- [88] H. J. Gwon, Y. Park, C. W. Moon, S. Nahm, S. J. Yoon, S. Y. Kim, H. W. Jang, *Nano Res.* **2014**, *7*, 670.
- [89] M. Tabata, I. Adachi, T. Fukushima, H. Kawai, H. Kishimoto, A. Kuratani, H. Nakayama, S. Nishida, T. Noguchi, K. Okudaira, *IEEE NSS/MIC*, IEEE, Fajardo, Puerto Rico **2005**.

- [90] B. E. Yoldas, D. P. Partlow, *Thin Solid Films* **1985**, 129, 1.
- [91] M. M. Braun, L. Pilon, *Thin Solid Films* **2006**, 496, 505.
- [92] D. Schwarz, H. Wormeester, B. Poelsema, *Thin Solid Films* **2011**, 519, 2994.
- [93] S. Eslava, M. R. Baklanov, C. E. Kirschhock, F. Iacopi, S. Aldea, K. Maex, J. A. Martens, *Langmuir* **2007**, 23, 12811.
- [94] D. Karthik, S. Pendse, S. Sakthivel, E. Ramasamy, S. V. Joshi, *Sol. Energy Mater. Sol. Cells* **2017**, 159, 204.
- [95] B. E. Yoldas, *Appl. Opt.* **1980**, 19, 1425.
- [96] G. D. Bernard, W. H. Miller, *Invest. Ophthalmol. Vis. Sci.* **1968**, 7, 416.
- [97] C. G. Bernhard, G. Gemne, J. Sällström, Z. Vgl. *Physiol.* **1970**, 67, 1.
- [98] P. Clapham, M. Hutley, *Nature* **1973**, 244, 281.
- [99] S. Wilson, M. Hutley, *J. Mod. Opt.* **1982**, 29, 993.
- [100] J. Cai, L. Qi, *Mater. Horiz.* **2015**, 2, 37.
- [101] Z. W. Han, Z. Wang, X. M. Feng, B. Li, Z. Z. Mu, J. Q. Zhang, S. C. Niu, L. Q. Ren, *Biosurf. Biotechnol.* **2016**, 2, 137.
- [102] S. Ji, J. Park, H. Lim, *Nanoscale* **2012**, 4, 4603.
- [103] Y. Hirabayashi, S. Kaneko, K. Akiyama, K. Sakurazawa, M. Yasui, *ECS Trans.* **2010**, 25, 69.
- [104] N. Das, S. I. Sen, AUPEC "Green Smart Grid Systems," IEEE, Bali, Indonesia **2012**.
- [105] O. Deparis, S. Mouchet, L. Dellieu, J. F. Colomer, M. Sarrazin, *Mater. Today: Proc.* **2014**, 1, 122.
- [106] M. Weismann, D. F. Gallagher, N. C. Panoiu, *J. Opt.* **2015**, 17, 125612.
- [107] M. T. Scholz, G. V. Tiers (3M Co), *US5585186A*, **1996**.
- [108] W. Shin, MATLAB-based solver package of Maxwell's equations by the FDFD method, <https://github.com/wsshin/maxwellfdtd> (accessed: September 2017).
- [109] How long do butterflies and moths live?, <http://www.butterfliesandmoths.org/faq/how-long-do-butterflies-and-moths-live> (accessed: February 2017).
- [110] X. Li, J. Gao, L. Xue, Y. Han, *Adv. Funct. Mater.* **2010**, 20, 259.
- [111] X. Cui, R. Ding, M. Wang, C. Zhang, C. Zhang, J. Zhang, Y. Xu, *Adv. Opt. Mater.* **2016**, 4, 722.
- [112] S. B. Khan, H. Wu, L. Ma, M. Hou, Z. Zhang, *Adv. Mater. Interfaces* **2017**, 4, 1600892.
- [113] U. Schulz, P. Munzert, F. Rickelt, N. Kaiser, *Thin Solid Films* **2013**, 532, 119.
- [114] E. E. Perl, W. E. McMahon, R. M. Farrell, S. P. Denbaars, J. S. Speck, J. E. Bowers, *Nano Lett.* **2014**, 14, 5960.
- [115] D. Chen, *Sol. Energy Mater. Sol. Cells* **2001**, 68, 313.
- [116] P. K. Biswas, P. Sujatha Devi, P. K. Chakraborty, A. Chatterjee, D. Ganguli, M. P. Kamath, A. S. Joshi, *J. Mater. Sci. Lett.* **2003**, 22, 181.
- [117] W. H. Lowdermilk, in *SPIE Radiation Effects in Optical Materials* (Ed: P. W. Levy), Vol. 0541, SPIE, Albuquerque, USA **1985**.
- [118] S. Singaravelu, D. C. Mayo, H. K. Park, K. E. Schriver, J. M. Klopff, M. J. Kelley, R. F. Haglund Jr., *Appl. Phys. A: Mater. Sci. Process.* **2014**, 117, 1415.
- [119] X. Fu, L. Dong, P. Lu, X. Fu, W. Duan, X. Li, R. Yin, *ICO20: Optical Design and Fabrication*, Vol. 6034, SPIE, China **2005**.
- [120] H. Merzendorfer, L. Zimoch, *J. Exp. Biol.* **2003**, 206, 4393.
- [121] Y. K. Fuh, C. C. Peng, C. T. Huang, *Nanoscale Res. Lett.* **2013**, 8, 1.
- [122] Z. Diao, M. Kraus, R. Brunner, J. H. Dirks, J. P. Spatz, *Nano Lett.* **2016**, 16, 6610.
- [123] R. Glass, M. Möller, J. P. Spatz, *Nanotechnology* **2003**, 14, 1153.
- [124] U. Schulz, *Appl. Opt.* **2006**, 45, 1608.
- [125] L. Yao, J. He, *Prog. Mater. Sci.* **2014**, 61, 94.
- [126] D. Stavenga, S. Foletti, G. Palasantzas, K. Arikawa, *Proc. R. Soc. London, Ser. B* **2006**, 273, 661.
- [127] P. Stoddart, P. Cadusch, T. Boyce, R. Erasmus, J. Cornins, *Nanotechnology* **2006**, 17, 680.
- [128] W. Barthlott, M. Mail, B. Bhushan, K. Koch, *Nano-Micro Lett.* **2017**, 9, 23.
- [129] A. Rodríguez-Palomo, E. Céspedes, D. Hernández-Pinilla, C. Prieto, *Sol. Energy Mater. Sol. Cells* **2018**, 174, 50.
- [130] C. J. Ting, F. Y. Chang, C. F. Chen, C. P. Chou, J. *Micro-mech. Microeng.* **2008**, 18, 075001.
- [131] K. C. Park, H. J. Choi, C. H. Chang, R. E. Cohen, G. H. McKinley, G. Barbasthis, *ACS Nano* **2012**, 6, 3789.
- [132] G. R. J. Artus, S. Jung, J. Zimmermann, H. P. Gautschi, K. Marquardt, S. Seeger, *Adv. Mater.* **2006**, 18, 2758.
- [133] M. Faustini, L. Nicole, C. Boissière, P. Innocenzi, C. Sanchez, D. Grosso, *Chem. Mater.* **2010**, 22, 4406.
- [134] C. H. Chen, S. Y. Li, A. S. T. Chiang, A. T. Wu, Y. S. Sun, *Sol. Energy Mater. Sol. Cells* **2011**, 95, 1694.
- [135] K. Sun, F. H. Saadi, M. F. Lichterman, W. G. Hale, H.-P. Wang, X. Zhou, N. T. Plymale, S. T. Ormelchenko, J.-H. He, K. M. Papadantonakis, *Proc. Natl. Acad. Sci. USA* **2015**, 112, 3612.
- [136] J. Zhu, L. Xu, J. He, *Chem. - Eur. J.* **2012**, 18, 16393.
- [137] R. F. Spaide, D. A. Orlock, B. Herrmann-Delemazure, A. P. Ciardella, L. A. Yannuzzi, K. B. Freund, Y. L. Fisher, D. R. Guyer, J. S. Slakter, J. A. Sorenson, *Retina* **1998**, 18, 44.
- [138] T. Gao, J. Lu, L. J. Rothberg, *Anal. Chem.* **2006**, 78, 6622.
- [139] S. Kim, U. T. Jung, S. K. Kim, J. H. Lee, H. S. Choi, C. S. Kim, M. Y. Jeong, *ACS Appl. Mater. Interfaces* **2015**, 7, 326.
- [140] Self-Cleaning Solar Panels Maximize Energy Efficiency, <http://www.asme.org/engineering-topics/articles/energy/self-cleaning-solar-panels-maximize-efficiency> (accessed: January 2018).
- [141] Nature Inspired Self-cleaning Windows Developed, <http://www.ucl.ac.uk/news/news-articles/0116/200116-self-cleaning-windows> (accessed: March 2018).
- [142] R. Blossy, *Nat. Mater.* **2003**, 2, 301.
- [143] M. Mani, R. Pillai, *Renewable Sustainable Energy Rev.* **2010**, 14, 3124.
- [144] M. Ma, R. M. Hill, *Curr. Opin. Colloid Interface Sci.* **2006**, 11, 193.
- [145] A. C. Zettlemoyer, in *Hydrophobic Surfaces* (Ed: F. M. Fowkes), Academic Press, New York, USA **1969**.
- [146] X. M. Li, D. Reinhoudt, M. Crego-Calama, *Chem. Soc. Rev.* **2007**, 36, 1350.
- [147] R. N. Wenzel, *Ind. Eng. Chem.* **1936**, 28, 988.
- [148] A. Marmur, *Langmuir* **2008**, 24, 7573.
- [149] A. Marmur, *Langmuir* **2003**, 19, 8343.
- [150] S. Ikegami, H. Kojyoh, I. Uchida, T. Yamazaki, T. Miyajima (Fuji Seal Inc, Kohjin Co Ltd), *US5376392A*, **1994**.
- [151] A. Razmjou, E. Arifin, G. Dong, J. Mansouri, V. Chen, *J. Membr. Sci.* **2012**, 415, 850.
- [152] V. A. Ganesh, H. K. Raut, A. S. Nair, S. Ramakrishna, *J. Mater. Chem.* **2011**, 21, 16304.
- [153] R. K. Gupta, P. Kumar, V. Yadav, S. Arora, D. P. Singh, S. K. Joshi, A. K. Chawla, A. Biswas, *Curr. Nanosci.* **2016**, 12, 429.
- [154] W. Chen, A. Y. Fadeev, M. C. Hsieh, D. Öner, J. Youngblood, T. J. McCarthy, *Langmuir* **1999**, 15, 3395.
- [155] T. Darmanin, F. Guittard, *Mater. Today* **2015**, 18, 273.
- [156] S. Nishimoto, B. Bhushan, *RSC Adv.* **2013**, 3, 671.
- [157] X. Du, Y. Xing, M. Zhou, X. Li, H. Huang, X. M. Meng, Y. Wen, X. Zhang, *Microporous Mesoporous Mater.* **2018**, 255, 84.
- [158] K. Koch, W. Barthlott, *Philos. Trans. R. Soc., A* **2009**, 367, 1487.
- [159] a) S. Banerjee, D. D. Dionysiou, S. C. Pillai, *Appl. Catal., B* **2015**, 176–177, 396; b) I. P. Parkin, R. G. Palgrave, *J. Mater. Chem.* **2005**, 15, 1689.
- [160] J. Drelich, E. Chibowski, *Langmuir* **2010**, 26, 18621.
- [161] a) K. Guan, *Surf. Coat. Technol.* **2005**, 191, 155; b) M. R. Hoffmann, S. T. Martin, W. Choi, D. W. Bahnemann, *Chem. Rev.* **1995**, 95, 69.
- [162] J. W. Wang, Y. C. Bai, W. Yao, H. N. Wang, R. Y. Chen, *Wuji Cailiao Xuebao [J. Inorg. Mater.]* **2011**, 26, 769.
- [163] X. Du, J. He, *J. Colloid Interface Sci.* **2012**, 381, 189.
- [164] X. Gao, X. Yan, X. Yao, L. Xu, K. Zhang, J. Zhang, B. Yang, L. Jiang, *Adv. Mater.* **2007**, 19, 2213.
- [165] C. Neinhuis, W. Barthlott, *Ann. Bot.* **1997**, 79, 667.

- [166] Y. Paz, Z. Luo, L. Rabenberg, A. Heller, *J. Mater. Res.* **1995**, *10*, 2842.
- [167] Pilkington Activ, <http://www.pilkington.com/north-america/USA/English/products/bp/bybenefit/selfcleaning/activ/default.htm> (accessed: February 2017).
- [168] Lotusan – für saubere und trockene Fassaden, <http://www.lotusan.de/de/produkte-mit-lotus-effect/produkte-mit-lotus-effect/produkte-lotus-effekt.html> (accessed: February 2017).
- [169] Neat Glass, <http://www.cardinalcorp.com/products/coated-glass/neat-glass/> (accessed: February 2017).
- [170] SUNCLEAN self-cleaning glass for commercial applications, <http://corporate.ppg.com/Media/Newsroom/2012/20121022B> (accessed: February 2017).
- [171] L. Feng, Y. Zhang, J. Xi, Y. Zhu, N. Wang, F. Xia, L. Jiang, *Langmuir* **2008**, *24*, 4114.
- [172] H. M. Shang, Y. Wang, S. J. Limmer, T. P. Chou, K. Takahashi, G. Z. Cao, *Thin Solid Films* **2005**, *472*, 37.
- [173] M. Sun, G. S. Watson, Y. Zheng, J. A. Watson, A. Liang, *J. Exp. Biol.* **2009**, *212*, 3148.
- [174] S. A. Boden, D. M. Bagnall, in *Encyclopedia of Nanotechnology* (Ed: B. Bhushan), 2012 ed., Springer, The Netherlands **2012**, Ch. M.
- [175] a) G. McHale, M. I. Newton, N. J. Shirtcliffe, *Soft Matter* **2010**, *6*, 714; b) P. Zhang, F. Y. Lv, *Energy* **2015**, *82*, 1068.
- [176] A. Lafuma, D. Quere, *Nat. Mater.* **2003**, *2*, 457.
- [177] R. N. Wenzel, *J. Phys. Chem.* **1949**, *53*, 1466.
- [178] A. Cassie, *Discuss. Faraday Soc.* **1948**, *3*, 11.
- [179] U. Mehmood, F. A. Al-Sulaiman, B. S. Yilbas, B. Salhi, S. H. A. Ahmed, M. K. Hossain, *Sol. Energy Mater. Sol. Cells* **2016**, *157*, 604.
- [180] D. Kontziampasis, G. Boulousis, A. Smyrnakis, K. Ellinas, A. Tserepi, E. Gogolides, *Microelectron. Eng.* **2014**, *121*, 33.
- [181] Y. Li, X. Men, X. Zhu, B. Ge, F. Chu, Z. Zhang, *J. Mater. Sci.* **2016**, *51*, 2411.
- [182] W. Dou, P. Wang, D. Zhang, J. Yu, *Mater. Lett.* **2016**, *167*, 69.
- [183] P. Ditsche-Kuru, E. S. Schneider, J. E. Melskotte, M. Brede, A. Leder, W. Barthlott, *Beilstein J. Nanotechnol.* **2011**, *2*, 137.
- [184] B. Dean, B. Bhushan, *Philos. Trans. R. Soc. A* **2010**, *368*, 4775.
- [185] G. D. Bixler, B. Bhushan, *Nanoscale* **2013**, *5*, 7685.
- [186] Speedo Fastskin Racing Swimsuits, <https://speedo.com.au/collections/racing-suits> (accessed: March 2017).
- [187] D. Trevallion, "Fast suits" and Olympic swimming: a tale of reduced drag and broken records, <http://theconversation.com/fast-suits-and-olympic-swimming-a-tale-of-reduced-drag-and-broken-records-7960> (accessed: June 2017).
- [188] a) T. Kobayashi, S. Konishi, *J. Micromech. Microeng.* **2015**, *25*, 115014; b) D. Tian, X. Zhang, Y. Tian, Y. Wu, X. Wang, J. Zhai, L. Jiang, *J. Mater. Chem.* **2012**, *22*, 19652.
- [189] P. Suresh Kumar, J. Sundaramurthy, D. Mangalaraj, D. Nataraj, D. Rajarathnam, M. P. Srinivasan, *J. Colloid Interface Sci.* **2011**, *363*, 51.
- [190] F. Xia, Y. Zhu, L. Feng, L. Jiang, *Soft Matter* **2009**, *5*, 275.
- [191] J. Gao, Y. Liu, H. Xu, Z. Wang, X. Zhang, *Langmuir* **2010**, *26*, 9673.
- [192] D. Wu, S. Z. Wu, Q. D. Chen, Y. L. Zhang, J. Yao, X. Yao, L. G. Niu, J. N. Wang, L. Jiang, H. B. Sun, *Adv. Mater.* **2011**, *23*, 545.
- [193] A. Tuteja, W. Choi, M. Ma, J. M. Mabry, S. A. Mazzella, G. C. Rutledge, G. H. McKinley, R. E. Cohen, *Science* **2007**, *318*, 1618.
- [194] H. Wang, Y. Xue, J. Ding, L. Feng, X. Wang, T. Lin, *Angew. Chem., Int. Ed.* **2011**, *50*, 11433.
- [195] C. Dutriez, K. Satoh, M. Kamigaito, H. Yokoyama, *Polym. J.* **2016**, *48*, 497.
- [196] X. Zhang, M. Lin, L. Lin, M. Zhuang, L. Ye, W. Yang, B. Jiang, *J. Sol-Gel Sci. Technol.* **2015**, *74*, 698.
- [197] F. Joki-Korpela, J. Karvinen, B. Päiväntanta, A. Partanen, M. Suvanto, M. Kuittinen, T. T. Pakkanen, *Microelectron. Eng.* **2014**, *114*, 38.
- [198] M. S. Khalil-Abad, M. E. Yazdanshenas, *J. Colloid Interface Sci.* **2010**, *351*, 293.
- [199] S. Pogodin, J. Hasan, V. A. Baulin, H. K. Webb, V. K. Truong, V. Boshkovikj, C. J. Fluke, G. S. Watson, J. A. Watson, R. J. Crawford, *Biophys. J.* **2013**, *104*, 835.
- [200] E. P. Ivanova, J. Hasan, H. K. Webb, G. Gervinskas, S. Juodkazis, V. K. Truong, A. H. Wu, R. N. Lamb, V. A. Baulin, G. S. Watson, *Nat. Commun.* **2013**, *4*, 2838.
- [201] S. A. Kulinich, S. Farhadi, K. Nose, X. W. Du, *Langmuir* **2011**, *27*, 25.
- [202] R. M. Fillion, A. R. Riahi, A. Edrissy, *Renewable Sustainable Energy Rev.* **2014**, *32*, 797.
- [203] S. Jung, M. Dorrestijn, D. Raps, A. Das, C. M. Megaridis, D. Poulikakos, *Langmuir* **2011**, *27*, 3059.
- [204] L. B. Boinovich, A. M. Emelyanenko, *Mendelev Commun.* **2013**, *23*, 3.
- [205] Y. Wang, J. Xue, Q. Wang, Q. Chen, J. Ding, *ACS Appl. Mater. Interfaces* **2013**, *5*, 3370.
- [206] P. Manoudis, I. Karapanagiotis, A. Tsakalof, I. Zuburtikudis, B. Kolinkeová, C. Panayiotou, *Appl. Phys. A: Mater. Sci. Process.* **2009**, *97*, 351.
- [207] F. Stranges, M. Barberio, P. Barone, A. Abenante, A. Leuzzi, P. Sapia, F. Xu, A. Bonanno, *Archaeol. Discovery* **2013**, *1*, 32.
- [208] G. J. Jorgensen, S. Brunold, M. Koehl, P. Nostell, H. Oversloot, A. Roos, *SPIE Int. Symp. on Optical Science, Engineering, and Instrumentation*, Vol. 3789, SPIE, CO, USA **1999**.
- [209] B. Chapman, *J. Vac. Sci. Technol.* **1974**, *11*, 106.
- [210] J. Malzbender, J. Den Toonder, A. Balkenende, G. De With, *Mater. Sci. Eng., R* **2002**, *36*, 47.
- [211] T. Hull, J. Colligon, A. Hill, *Vacuum* **1987**, *37*, 327.
- [212] R. Jacobsson, *Thin Solid Films* **1976**, *34*, 191.
- [213] L. Y. Wu, E. Chwa, Z. Chen, X. Zeng, *Thin Solid Films* **2008**, *516*, 1056.
- [214] C. M. Stafford, C. Harrison, K. L. Beers, A. Karim, E. J. Amis, M. R. VanLandingham, H.-C. Kim, W. Volksen, R. D. Miller, E. E. Simonyi, *Nat. Mater.* **2004**, *3*, 545.
- [215] X. Du, Y. Xing, X. Li, H. Huang, Z. Geng, J. He, Y. Wen, X. Zhang, *RSC Adv.* **2016**, *6*, 7864.
- [216] X. Deng, L. Mammen, Y. Zhao, P. Lellig, K. Müllen, C. Li, H. J. Butt, D. Vollmer, *Adv. Mater.* **2011**, *23*, 2962.
- [217] L. Xu, J. He, *J. Mater. Chem. C* **2013**, *1*, 4655.
- [218] a) T. K. Boström, E. Wäckelgård, G. Westin, *Sol. Energy Mater. Sol. Cells* **2005**, *89*, 197; b) J. Cai, J. Ye, S. Chen, X. Zhao, D. Zhang, S. Chen, Y. Ma, S. Jin, L. Qi, *Energy Environ. Sci.* **2012**, *5*, 7575; c) K. Cathro, D. Constable, T. Solaga, *Sol. Energy* **1981**, *27*, 491; d) M. Sakhuja, J. Son, H. Yang, C. S. Bhatia, A. J. Danner, *Sol. Energy* **2014**, *110*, 231; e) X. Wang, J. Shen, *J. Sol-Gel Sci. Technol.* **2010**, *53*, 322.
- [219] L. Xu, Z. Geng, J. He, G. Zhou, *ACS Appl. Mater. Interfaces* **2014**, *6*, 9029.
- [220] T. Verho, C. Bower, P. Andrew, S. Franssila, O. Ikkala, R. H. Ras, *Adv. Mater.* **2011**, *23*, 673.
- [221] R. A. Taylor, Y. Hewakuruppu, D. Dejarnette, T. P. Otanicar, *Appl. Opt.* **2016**, *55*, 3829.
- [222] Antireflection (AR) Coated High Efficiency Windows – Product code: 43-975, <https://www.edmundoptics.com.au/optics/windows-diffusers/visible-windows/anti-reflection-ar-coated-high-efficiency-windows/> (accessed: May 2017).
- [223] Specialty Glass Substrates – OptiView Antireflective Glass, <http://www.viracon.com/page/substrates> (accessed: May 2017).
- [224] R. Brunner, O. Sandfuchs, C. Pacholski, C. Morhard, J. Spatz, *Laser Photonics Rev.* **2012**, *6*, 641.
- [225] L. Peng, C. Zhang, H. Wu, P. Yi, X. Lai, J. Ni, *IEEE Trans. Nano-technol.* **2016**, *15*, 971.
- [226] S. A. Boden, D. M. Bagnall, *SPIE Nanoscience + Engineering*, Vol. 7401, SPIE, CA, USA **2009**.

- [227] J. W. Leem, B. Dudem, J. S. Yu, *RSC Adv.* **2016**, 6, 79755.
- [228] C. M. Lung, W. C. Wang, C. H. Chen, L. Y. Chen, M. J. Chen, *Mater. Chem. Phys.* **2016**, 180, 195.
- [229] L. Xiao, Y. Lv, W. Dong, N. Zhang, X. Liu, *ACS Appl. Mater. Interfaces* **2016**, 8, 27107.
- [230] G. D. Bixler, B. Bhushan, *Adv. Funct. Mater.* **2013**, 23, 4507.
- [231] Z. She, Q. Li, Z. Wang, L. Li, F. Chen, J. Zhou, *Chem. Eng. J.* **2013**, 228, 415.
- [232] A. L. Olsen, W. R. McBride, *J. Opt. Soc. Am.* **1963**, 53, 1003_1.
- [233] Y. Li, S. Ren, *Building Decorative Materials*, Woodhead Publishing Limited, Cambridge, UK **2011**.
- [234] M. Ibn-Elhaj, M. Schadt, *Nature* **2001**, 410, 796.
- [235] D. Lee, M. F. Rubner, R. E. Cohen, *Nano Lett.* **2006**, 6, 2305.
- [236] C.-H. Chan, A. Fischer, A. Martinez-Gil, P. Taillepiere, C.-C. Lee, S.-L. Yang, C.-H. Hou, H.-T. Chien, D.-P. Cai, K.-C. Hsu, *Appl. Phys. B* **2010**, 100, 547.
- [237] L. Cao, D. Gao, *Faraday Discuss.* **2010**, 146, 57.
- [238] S. H. Lee, K. S. Han, J. H. Shin, S. Y. Hwang, H. Lee, *Prog. Photo-voltaics* **2013**, 21, 1056.
- [239] H. G. Craighead, R. E. Howard, J. E. Sweeney, D. M. Tennant, *J. Vac. Sci. Technol.* **1982**, 20, 316.
- [240] G. P. Montgomery Jr., *Opt. Eng.* **1982**, 21, 1039.
- [241] J. Strumpf, G. Beister, D. Schulze, M. Kammer, S. Rehn, in *Annual Technical Conf. Proc. of the Society of Vacuum Coaters*, (Ed.: V. H. Mattox), Vol. 40, Society of Vacuum Coaters, Albuquerque, New Orleans, USA **1997**.
- [242] J. Gottmann, E. W. Kreutz, *Surf. Coat. Technol.* **1999**, 116–119, 1189.
- [243] H. Ishikawa, Y. Honjo, K. Watanabe, *Thin Solid Films* **1999**, 351, 212.
- [244] M. Mennig, P. W. Oliveira, H. Schmidt, *Thin Solid Films* **1999**, 351, 99.
- [245] P. Belleville, P. Prené, *XIII Int. Symp. on Gas Flow and Chemical Lasers and High-Power Laser Conf.*, Vol. 4184, SPIE, Florence, Italy **2001**.
- [246] P. Frach, D. Gloess, H. Bartsch, K. Taeschner, J. Liebig, E. Schultheiss, *Thin Solid Films* **2010**, 518, 3105.
- [247] M. Yuste, R. E. Galindo, S. Carvalho, J. M. Albella, O. Sánchez, *Appl. Surf. Sci.* **2011**, 258, 1784.
- [248] K. H. Choi, H. W. Koo, T. W. Kim, H. K. Kim, *Appl. Phys. Lett.* **2012**, 100, 263505.
- [249] X. Li, J. He, W. Liu, *Mater. Res. Bull.* **2013**, 48, 2522.
- [250] J. Y. Y. Loh, D. P. Puzzo, P. G. O'Brien, G. A. Ozin, N. P. Kherani, *RSC Adv.* **2014**, 4, 31188.
- [251] J. H. Lu, T. W. Huang, C. Y. Cheng, J. W. Lee, C. W. Chang, *J. Vac. Sci. Technol. A* **2016**, 34, 051513.
- [252] K. Marszałek, A. Małek, P. Winkowski, *Opt. Appl.* **2016**, 46, 187.
- [253] T. X. Lin, F. M. Hsu, Y. L. Lee, R. Goseki, T. Ishizone, J. S. Jan, *ACS Appl. Mater. Interfaces* **2016**, 8, 26309.
- [254] Y. Fang, G. Sun, T. Wang, Q. Cong, L. Ren, *Chin. Sci. Bull.* **2007**, 52, 711.
- [255] S.-H. Kang, T.-Y. Tai, T.-H. Fang, *Curr. Appl. Phys.* **2010**, 10, 625.
- [256] J. Zi, X. Yu, Y. Li, X. Hu, C. Xu, X. Wang, X. Liu, R. Fu, *Proc. Natl. Acad. Sci. USA* **2003**, 100, 12576.
- [257] I. Badge, A. Y. Stark, E. L. Paoloni, P. H. Niewiarowski, A. Dhinojwala, *Sci. Rep.* **2014**, 4, 6643.
- [258] S. Han, S. Ji, A. Abdullah, D. Kim, H. Lim, D. Lee, *Appl. Surf. Sci.* **2018**, 429, 244.
- [259] Y. Li, K. Yang, B. Xia, B. Yang, L. Yan, M. He, H. Yan, B. Jiang, *RSC Adv.* **2017**, 7, 14660.
- [260] B. Jin, J. He, L. Yao, Y. Zhang, J. Li, *ACS Appl. Mater. Interfaces* **2017**, 9, 17466.
- [261] J. Chen, L. Zhang, Z. Zeng, G. Wang, G. Liu, W. Zhao, T. Ren, Q. Xue, *Colloids Surf., A* **2016**, 509, 149.
- [262] X. Ye, X. Jiang, J. Huang, F. Geng, L. Sun, X. Zu, W. Wu, W. Zheng, *Sci. Rep.* **2015**, 5, 13023.
- [263] L. Yao, J. He, *J. Mater. Chem. A* **2014**, 2, 6994.
- [264] L. Yao, J. He, *Langmuir* **2013**, 29, 3089.
- [265] X. Li, J. He, *ACS Appl. Mater. Interfaces* **2013**, 5, 5282.
- [266] A. N. Parikh, D. L. Allara, I. B. Azouz, F. Rondelez, *J. Phys. Chem.* **1994**, 98, 7577.
- [267] M. Psarski, J. Marczak, G. Celichowski, G. Sobieraj, K. Gumowski, F. Zhou, W. Liu, *Open Phys.* **2012**, 10, 1197.
- [268] P.-S. Tsai, Y.-M. Yang, Y.-L. Lee, *Nanotechnology* **2007**, 18, 465604.
- [269] J. X. Wong, H. Asanuma, H.-Z. Yu, *Thin Solid Films* **2012**, 522, 159.
- [270] C.-T. Hsieh, F.-L. Wu, W.-Y. Chen, *Mater. Chem. Phys.* **2010**, 121, 14.
- [271] T. Wang, T. T. Isimjan, J. Chen, S. Rohani, *Nanotechnology* **2011**, 22, 265708.
- [272] H. Sugimura, A. Hozumi, T. Kameyama, O. Takai, *Surf. Interface Anal.* **2002**, 34, 550.
- [273] M. Zhang, S. Wang, C. Wang, J. Li, *Appl. Surf. Sci.* **2012**, 261, 561.
- [274] X. Song, J. Zhai, Y. Wang, L. Jiang, *J. Colloid Interface Sci.* **2006**, 298, 267.
- [275] Ceramic Pro Rain – Superhydrophobic Coating for Glass Surfaces, <http://ceramic-pro.com/en/shop/product-line/product/rain/> (accessed: February 2017).
- [276] Aquapel Applicator Pack, <http://www.aquapel.com/Aquapel-retail-pack.php> (accessed: February 2017).
- [277] Rust-Oleum NeverWet Liquid Repelling Treatment, <http://www.rustoleum.com.au/product-catalog/consumer-brands/neverwet/neverwet-kit> (accessed: February 2017).
- [278] Hydrobead - Super Water Repellent Spray, <http://www.hydrobead.com/consumer> (accessed: February 2017).
- [279] C. Tao, H. Yan, X. Yuan, Q. Yin, J. Zhu, W. Ni, L. Yan, L. Zhang, *J. Sol-Gel Sci. Technol.* **2016**, 80, 10.
- [280] D. Ebert, B. Bhushan, *Langmuir* **2012**, 28, 11391.
- [281] D. H. Kim, J. H. Park, T. I. Lee, J. M. Myoung, *Sol. Energy Mater. Sol. Cells* **2016**, 150, 65.
- [282] Y. C. Chen, Z. S. Huang, H. Yang, *ACS Appl. Mater. Interfaces* **2015**, 7, 25495.
- [283] H. K. Raut, *PhD Thesis*, National University of Singapore **2014**.